To the Graduate Council:

I am submitting herewith a dissertation written by Cyrus Aghanajafi entitled "Ionospheric Total Electron Content, and Far Ultraviolet, Near Infrared Oxygen Emission." I have examined the final copy of this dissertation for form and content and recommend that it be accepted in partial fulfillment of the requirements for the degree of Doctor of Philosophy, with a major in Mechanical Engineering.

F. Shahrokhi, Major Professor

We have read this dissertation
and recommend its acceptance:

Accepted for the Council:

Vice Provost
and Dean of the Graduate School

IONOSPHERIC TOTAL ELECTRON CONTENT, AND FAR ULTRAVIOLET, NEAR INFRARED OXYGEN EMISSION

A Dissertation

Presented for the

Doctor of Philosophy

Degree

The University of Tennessee, Knoxville

Cyrus Aghanajafi

December 1988

ACKNOWLEDGEMENT

As is with any endeavor, I am indebted and grateful to the many people who have helped me directly and indirectly during my graduate work and in my life in general.

I am understandabely indebted to my supervisor Professor F. Shahrokhi for his help and unsurpassed technical knowledge in the field of remote sensing. I can honestly say he taught me more than just practical applied field engineering. Also, he was a father throughout my PhD program. I am also indebted to Professor Robert L. Young for his guidance as my advisor. His constant efforts and encouragment made it a Pleasure to study at The University of Tennessee Space Institute. Special thanks to Professor Walter Frost for his wonderful lectures in mechanical engineering department. I enjoyed any time that I attended in his classes. Special appreciation to Professor K. C. Reddy for helping me in mathematics. Without his notes, I was lost. Special thanks extended to Capitan. Joe Miller for providing me the code from Hanscom Air Force Laboratory. Special Appreciation to UTSI staff, Mrs. Callie Taylor at admission office, Mrs. Mary Lo at library, Mr. David Modeste, Ms. Lisa Blanks at graphic office and UTSI adminstration for giving me more computer time.

It is unlikely that anyone would persist at this goal without the full support of his parents. Moreover, it is unlikely that the ultimate purpose of this goal can ever be realized without such continued support. It is for past proof and future faith in his encouragement this dissertation is dedicated to the author's father, General Habib Aghanajafi. I also wish to thank my brother Sohrab, my sisters Soodabeh and Soraya Aghanajafi for continoues support throughout my PhD program.

ABSTRACT

The purpose of this investigation is to calculate the total electron content and four oxygen emissions for solar cycle maximum at equinox season. The investigation shows that the total electron content reaches its maximum development at 2100 LT with the crest nearest to the equator being the greatest. This asymmetry reverses at 0200 LT when the crest farthest from the equator is smallest. In spite of the fact that while N_{max} decreases at noon, and the layer becomes greater in altitude under the influence of the upward drift, the noon bite out occurs at the equator around 1200 LT.

The behavior of OI 6300$\mathring{A}$, the brightest dayglow source is investigated. The oxygen at 6300$\mathring{A}$ is strongly a function of N_{max} and h_{max}. The data for the OI 6300$\mathring{A}$ reveal that the latitudinal asymmetry is associated with the asymmetry in altitude of F_2 peak. The maximum electron density height is strongly affected by vertical $\overline{E} \times \overline{B}$ drift velocity. The emission at 1356$\mathring{A}$ and 7774$\mathring{A}$ is calculated using the radiative recombination and ion-ion recombination processes. The ion-ion recombination has substantial effect in total emission rates. The intensity of OI 911$\mathring{A}$ due to direct recombination to the ground state is obtained. These emissions can be used as a way of remotely sensing the F region and exosphere plasma properties, and the winds responsible for plasma transport.

TABLE OF CONTENTS

CHAPTER		PAGE
1.	INTRODUCTION	1
	1.1 F LAYER AND EXOSPHERE PLASMA	1
	1.2 EQULIBRIUM IN THE UPPER ATMOSPHERE	3
	1.3 ELCTRONIC STRUCTURE	4
	1.4 VARIATIONS IN THE IONOSPHERE	5
	1.5 PERTUBATIONS OF IONOSPHERE	6
	1.6 OPTICAL PHENOMENA	7
	1.7 ELECTRIC CURRENTS	8
	1.8 ANOMALIES	8
	1.9 THERMAL PROPERTIES	9
	1.10 PRODUCTION DETAILS	10
2.	LITERATURE SURVEY	12
	2.1 THE MODEL OF HARRIS AND PRIESTER	12
	2.2 LOW LATITUDE IONOSPHERIC MODEL	14
	2.3 EMISSION OF OXYGEN AT 6300$\AA$	21
	2.4 EMISSIONS OF OXYGEN AT 7774$\AA$, 1356$\AA$ AND 911$\AA$	23
	2.5 PERTUBATIONS IN RADIO SIGNALS	24
3.	ANALYTIC APPROACH	26
	3.1 CHAPMAN FUNCTION	26
4.	GENERAL ANALYSIS	29
	4.1 CHEMICAL RATE ANALYSIS TECHNIQUE	29
	4.2 THE SEMI EMPIRICAL IONOSPHERIC APPROACH	31
	4.3 VOLUME AND COLUMN EMISSION RATE OF OXYGEN	33

5. DISCUSION OF RESULTS 35
5.1 ELECTRON CONTENT 35
5.2 EMISSION RATE OF OXYGEN AT 6300Å 45
5.3 EMISSION RATES OF OXYGEN AT 1356Å AND 7774Å . 58
5.4 EMISSION OF OXYGEN AT 911Å 66
CHAPTER 6. CONCLUSION 68
CHAPTER 7. RECOMMENDATIONS 71
BIBLIOGRAPHY 72
VITA 79

LIST OF FIGURES

FIGURE		PAGE
1.1	Schematic Representation Of Atmospheric Regions	2
2.1	Ion-Neutral And Electron-Neutral Temperature Ratios As a Function Of Latitude	17
2.2	Upward $\overline{E} \times \overline{B}$ Drift Velocity Versus Time At Equinox Season	18
2.3	Contoure Plots Of Meridional Winds Versus Latitude At Equinox Season	19
4.1	A Comparison Between the Modified Chapman Model and Low Latitude Ionospheric Model (LLIM) at 0500 LT and 2000 LT	32
5.1	Total Electron Content Versus Magnetic Latitude For Sunspot Maximum At Equinox Season	36
5.2	Maximum Electron Density Height Versus Magnetic latitude For Sunspot Maximum At Equinox Season	41
5.3	Column Emission Of Oxygen At 6300ÅVersus Magnetic Latitude Sunspot Maximum At Equinox Season	46
5.4	Equatorial Volume Emission Rate Of Oxygen At 6300$\mathring{A}$ Versus Altitude For Sunspot Maximum At Equinox Season	53
5.5	Volume Emission Rate Of Oxygen At 6300$\mathring{A}$ Versus Altitude For Sunspot Maximum, Equinox Season At 0500 LT	56
5.6	Volume Emission Rate Of Oxygen At 6300$\mathring{A}$ Versus Altitude For Sunspot Maximum, Equinox Season At 0600 LT	57
5.7	Equatorial Volume Emission Rate Of Oxygen At 1356$\mathring{A}$ Versus Altitude For Sunspot Maximum At Equinox Season	60

5.8 The Dependence of the OI 1356$\AA$ Intensity on the N_{max} 61
5.9 Equatorial Volume Emission Rate Of Oxygen At 7774$\AA$
Versus Altitude For Sunspot Maximum At Equinox Season 63
5.10 Equatorial Volume Emission Rate Of Oxygen At 911$\AA$
Versus Altitude For Sunspot Maximum At Equinox Season 67

CHAPTER 1

INTRODUCTION

1.1 F LAYER AND EXOSPHERE PLASMA

The ionosphere is generally divided into six altitude regions designated as C, D, E, F_1, F_2 and exosphere plasma (Fig 1.1). In recent years F region and exosphere becomes very significant scientifically and technologically because of radar facility installation across The United States, nuclear explosion tests, and installation of space station in the F layer. The upper atmosphere explored by sattelites and radio sounding technique. The largest ionosphere layers are found to be the F layer and the exosphere plasma which produce multiple ecohes, presumably by reflection of radio signals. The outermost portion of the atmosphere which is almost ionized and where helium and hydrogen ions predominate is called the protonosphere by some and the exosphere by others, depending on whether they are emphasizing the ionic or neutal composition. The neutral gases present at these high altitudes constitute a screen which removes radiations harmful to life, and the partially ionized gas or plasma is closely associated with long distance radio communications and geomagnetic variations. The source of ionization includes both electromagnetic and corpuscular radiation. The energy emitted by the sun in the spectrum below 1500$\mathring{A}$ is, only approximately 10^{-5} the energy emitted over the entire spectrum. This insignificant energy has profound effects: it is responsible for the ionized state of the upper atmosphere and this provides the means for worldwide radio communication. On the other hand, an increase in flux of less than an order of magnitude in the solar X ray spectrum can make communications impossible in many frequency bands.

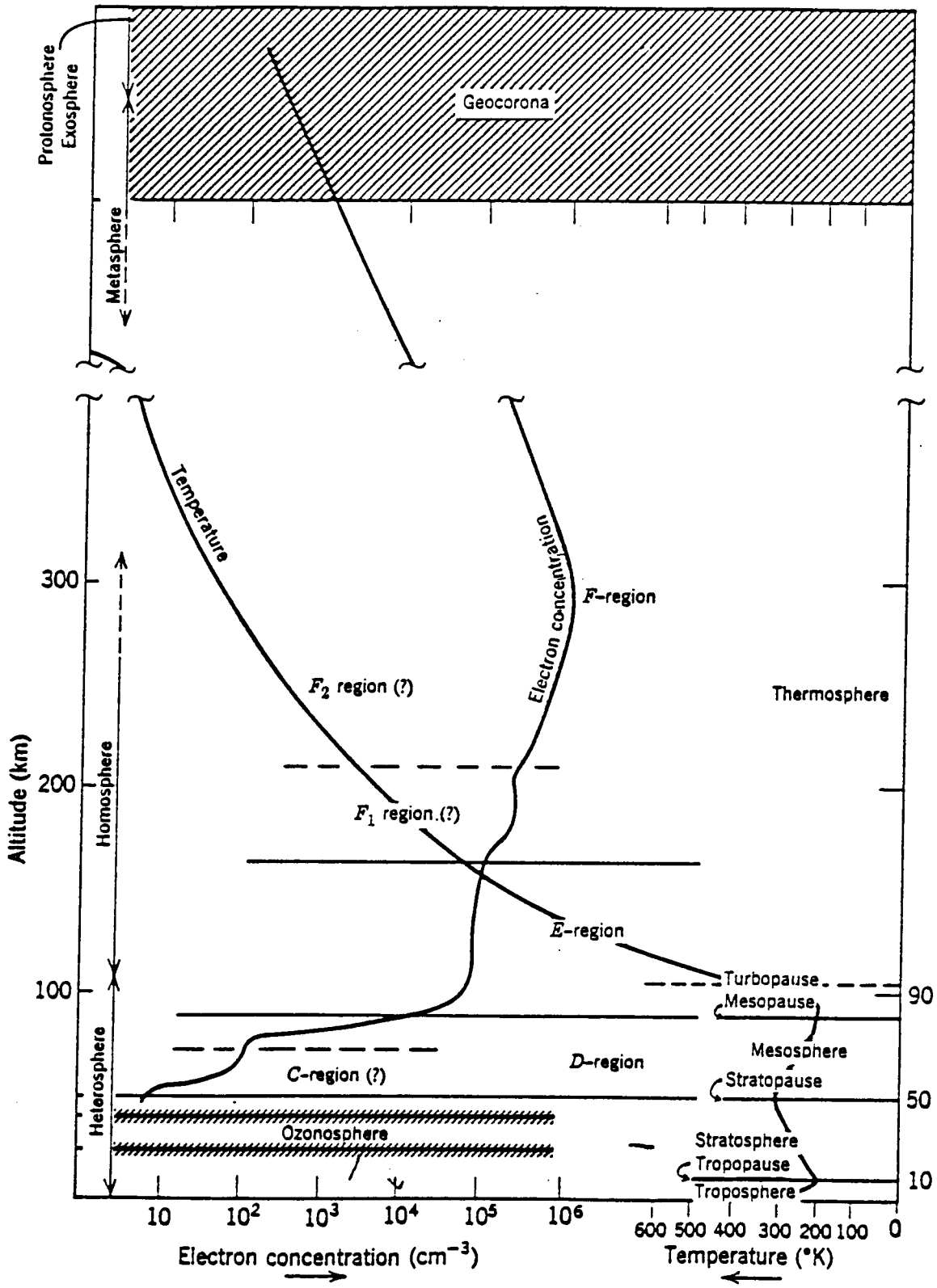


Figure 1.1 :Schematic representation of atmospheric regions.

The uniqe characteristic of the F_1 layer (180km-250km) is that the principal ions produced is atomic, whereas the principal electron disappearance process is dissociative recombination with a molecule ion. Thus, ion interchange is the key process that characterizes the F_1layer. On the other hand, it should be noted that ambipolar diffusion which is the diffusion rate of the ions through neutral gas across the field line is not important yet. At an altitude 250 km ambipolar diffusion becomes very significant which is called as F_2 layer. In the F_2 region itself the dominant ion is O^+ ,However, at higher altitudes $H^+$is present in greater concentrations.

The exosphere can be described as the region where the mean free path of the molecule is large and molecules move on ballistic trajectories and only very occasionally collide with each other. For typical exospheric temperatures and densities in the earth's upper atmosphere, about 550 km can be taken as the lower boundary of the exosphere.

For our investigations, the boundary between the low and, middle latitude regions defined as the latitude below which the significant equatorial EDP enhancements occur (Appleton anomaly), and significant irrequlariti̇es characteristic of the equatorial region such as spread F are found.

1.2 EQUILIBRIUM IN THE UPPER ATMOSPHERE

There are three types of equilibrium among the constituents that we must consider, depending upon the component in question as well as the altitude range. In the thermosphere one finds a condition of gravitational separation ,somtimes called diffusive equilibrium, above 120 km for all atmospheric constituents. At these levels the molecules move as independent particles. Each component obeys a hydrostatic law characterized by its own molecule mass with result that each

component also has its own hydrostatic equations and scale height which hold for each component separately.

At an altitude between 100 and 130 km (lower part of E region) molecular diffusion is dominated by atmopheric turbulance which leads to a mixing of the various components.

The last type of equilibrium is the photochemical equilibrium regime in which chemical productions and loss processes are much faster than molecular and eddy diffusion(C and D region).

1.3 ELECTRONIC STRUCTURE

The electronic structure of atoms and ions depend on atomic number and the energy associated with that orbit. Orbitals are filled with electrons in order of increasing energies. The s orbit can hold a maximum of two electrons, the p orbit can hold a total of six electrons, and the d orbit can hold a total of ten electrons. The p orbit has three sub shell, and the d orbit has five sub shells. When electrons are added to orbitals of the same energy (such as 3p orbitals), one electron enters each of the available orbitals before a second electron enters any one orbital. If the net charge from the nucleus and the filled inner orbitals were concentrated at a point at the nucleus, then the shell energies such as 3s, 3p, 3d orbitals would be the same. But the screening electrons extend over an appreciable volume of space.

The net attraction that an electron with a principal quantum number experiences depends on how close it comes to the nucleus, and whether it penetrates the lower screening electron clouds. As in Sommerfeld's elliptical orbit model, the s orbital comes closer to the nucleus, and is somewhat more stable than the p,and the p is more stable than the d. For a given value of the principal quantum number.

the order of increasing energy is s, p, d, f, g. Something unusual happens in the fourth period of the periodic table. The 4s orbital penetrates closer to the nucleus than does the 3d orbital,and at this point in the build up process the 4s has slightly lower energy than 3d.

Atomic numbers for N, O^{++}, Na are 7, 6, 11 respectively, and their atomic configurations are as following:

$$N = (1s)^2, (2s)^2, (2p_x)^1, (2p_y)^1, (2p_z)^1$$

$$O^{++} = (1s)^2, (2s)^2, (2p_x)^1, (2p_y)^1, (2p_z)^0$$

$$Na = (1s)^2, (2s)^2, (2p)^6, (3s)^1$$

Atomic structure changes significantly in different reactions. Electrons can move from one orbit to another and leave the atomic structure in the excited state. Depending on the life time of the exitation state, the atomic structure decays to the ground state through a cascading effect.

1.4 VARIATIONS IN THE IONOSPHERE

Variations in ionosphere structure, density, pressure, and temperature have their origin in the rotation of the earth(diurnal variations) , revolution of the earth about the sun (seasonal variations), and the sunspot cycle(solar cycle variations). In addition, these physical properties also depend upon geographic and magnetic latitudes.

The diurnal variations caused entirely by variation of the heating rate due to change in the flux of solar ultraviolet radiation. Although most of this radiation is absorbed at altitudes below the F_1 layer the amplitude of the density and temperature variations is small at these heights because of the large heat capacity of

the atmosphere. Higher in the thermosphere the heat capacity is smaller and daily fluctuations are greater.

Seasonal variations occur because of changes in the noon zenith angle as well as in the duration of daylight.

Solar activity has a very significant influence on upper atmosphere properties. Most of the effect is due to variations in the intensity of ultraviolet solar radiation incident on the earth. There is strong correlation between solar radio flux(Jansky)at wavelengths of 8 to 10.7 cm, the Zurich sun spot number, and upper atmosphere properties. The correlation of the 27 day (solar rotational period) average of radio flux at 10.7 cm with the 27 day average sunspot number(Wolf sunspot number) is more significant than the correlation of the instantaneous values. Because of the dependace of thermospheric temperatures on the solar heating rate, a linear relationship was suggested between solar cycle and temperatures.

1.5 PERTURBATIONS OF IONOSPHERE

Phenomena of a collective nature such as winds and waves are exteremly important in upper atmosphere. In particular these are acoustic gravity waves, atmospheric tides, winds, circulations and turbulent transport.

Thermospheric winds are the result of thermally created tidal motions at high altitudes. such air motions have ionospheric effects because of viscous interaction between atmosphere and ionosphere. In particular they raise or depress the altitude of the electron density peak. They also have pronounced effect on number densities of neutral components and on heat flow in the thermosphere.

Internal gravity waves are disturbances which propagate as a consequence of buoyant forces present in E region. Gravity waves which originate in the lower

atmosphere penetrate to the upper atmosphere with larger amplitude.

Tidal oscillations occur in atmospheric pressure at low altitude. These motions are responsible for the flow of electric currents in the ionosphere. These disturbances with large scale random fluctuations in density and velocity(turbulance) mix the atmosphere and cause instability in parts of the ionosphere.

1.6 OPTICAL PHENOMENA

Two types of optical phenomena occur in the upper atmosphere: auroras, and airglow. Airglow consists of dayglow, nightglow, twilight.

Dayglow is the result of excitation of atmospheric costituents by solar radiation and, to smaller extent, by low energy electrons. The main emission mechanism is resonance scattering which is the absorption of photons without a change in the photon energy and wavelength.

Twilight glow is a transition period between dayglow and nightglow. The emission mechanism is fluorescence which is the absorption of photons of one energy and the emission of photons of lesser energy; radiation of one wavelength is absorbed and radiation of a longer wavelength is emitted.

Nightglow phenomena are mainly produced by sunlight;they originate during the daylight and persist throughout the night. Solar radiation is, in essence, stored in dissociative, ionized,and excited species during the daytime and released at night by various relaxation processes such as ionic recombination,quantum emission, etc(chemiluminescence).

Auroras result from the energy dissipated by charged particles that bombard the atmosphere. The frequency of occurance decrease to minimum over the magnetic poles.

1.7 ELECTRIC CURRENTS

The requlars diurnal variations in the geomagnetic field are due to electric currents flowing in the upper atmosphere. Air motion caused by atmospheric tides sweeps the ions and electrons across the magnetic field lines. This induces electric fields which in turn produce the current flow. According to the dynamo theory, tidal winds produce the motion of the charged particles. Under quiet condition these winds and their associated currents can be seperated into two components, one due to solar and the other due to lunar variations.

1.8 ANOMALIES

There are several anomalies in the F_2 region such as electromagnetic drifts, nocturnal ionization, geographical anomalies, temporal anomalies and other irrequlars such as spread F. Electromagnetic drifts play a very important role at low geomagnetic latitude. Electric fields cause drifts across the geomagnetic field lines in the F_2 region. In addition, motions of the neutral atmosphere can induce currents by viscous drag. Such convection currents can have pronounced effect on the diurnal variation of maximum electron density, particularly in the equatorial F_2 layer.

It has been found that the F_2 region does not disappear at night, but rather falls to some quasi-equilibrium profile. Electron number density varies only slightly following the post sunset decrease. As may be expected, thermal contraction of the atmosphere and downward diffusion of electrons and ions will help to maintain the F_2 region at night. However, downward diffusion apparently cannot by itself account for the maintanace of the nocturnal F_2 layer, therefore, there is some source of ionization at night.

Geographical anomalies are undoubtedly a consequence of geomagnetic control of the F_2 region. The most striking geographic anomaly is the equatorial anomaly or (Appleton anomaly).

Temporal anomalies are diurnal, seasonal, annual. Ever since their causes are not known, for example near the equator noon bite out occurs which is depression in electron density distibutions.

There are several irrequlariti̇es present in the upper atmosphere such as spread F. large scale irrequlariti̇es associated with variations in the fading period of radio waves from a sattelite and radio star scintillation, or fluctuations in the observed amplitude of the radio waves from strongly emitted star.

Spread F is the reflection of a vertically incident electromagnetic wave and appears to occur at a continuum of altitudes. It occurs with greatest frequency at the equatorial region and high altitudes.

1.9 THERMAL PROPERTIES

The rather strong absorption of solar ultraviolet radiation in the F_2 region results in intense heating of the upper atmosphere. It has been found that even a small heat input to the electron gas must result in substantial departure from the thermal equilibrium in the ionosphere above 150 km. Because the photoelectrons rapidly thermalize with the ambient electron gas, they constitute a heat source for this gas. Energy is lost from the ambient electrons to the neutral particles and ions by elastic and inelastic collisions; it is also spatially redistributed by transport(heat conduction)so that equilibrium temperature at any given height is set by the rates of the heat input,loss, and conductive transfer. The temperature of the ion gas is established in similar manner; the heat input occurs via Rutherford scattering of

hot electrons, loss through elastic scattering of neutral particles, and transport by means of conduction. Hence, the electron temperature is substantially higher than that of the neutral atmosphere, and the ion temperature is in intermediate between the two.

1.10 PRODUCTION DETAILS

The Chapman profiles developed in the earliest days of ionospheric physics offer a simple way to explain the structure of the plasma in the upper atmosphere. They are based on relatively simple physics and thus can not be used to represent the entire electron density distributions that emerge from the more sophisticated simulation techniques in use today. As simple matematical formulas, however, they are well suited for representing portions of the ionospheric profile. Specially, while a single Chapman profile can not fit the entire $Ne(h)$, seperate formulas can be derived to investigate the significant parameters in upper atmosphere .

Unfortunately there are not enough data to generate the real EDP versus, altitude, latitude, time, season, solar cycle activity, therefore , another method is used to reproduce the topside and bottemside components of the peak electron density profiles with good results. It was decided to define a generalized Chapman formula with coefficents that vary for each topside and bottemside of the $Ne(h)$ profile. The total electron content is obtained by integrating the modified Chapman function to investigate the properties of the upper atmosphere, ionospheric bublles for solar cycle maximum, equinox season at exospheric temprature $1200^{\circ}K$.

Volume and column emission rates for four features of atomic oxegen are calculated using the modified Chapman function. The $6300\mathring{A}$ oxygen red line, arising from the intercombinational of magnetic dipole ^3P-^1D is one of the brithest day-

glow sources. The source of ^1D state is thought to be recombination of $NO^+$and O_2^+ with electrons, the photodissociation of O_2 by absorption of solar radiation in the Schumann Runge bands, and excitation by photoelectrons.

Volume and column emission rates of oxegen at 1356$\mathring{A}$ and 7774$\mathring{A}$ are calculated by using two excitation mechanisms.

1. Radiative recombination
2. Ion-Ion recombination

In Ion-Ion recombination, the atomic oxygen products may reside in excited states that directly or indirectly end in the ground states.

Particle precipitation has not been included in our calculations , because the problem with particle precipitation is that any exciting electrons would have to have an energy of about 10 ev to produce the right ratios of spectral line densities and to fail to excite lower altitude constituents such as molecular nitrogen.

The radiative recombination O^++ e will produce continua near 2772$\mathring{A}$,3026$\mathring{A}$ and a continuum near 910$\mathring{A}$ emission. The 911$\mathring{A}$ oxygen is direct recombination to the ground state. The column and volume emission rates of oxygen at 911$\mathring{A}$ are calculated. The calculations of oxygen intensities in far ultraviolet and near infrared provide a new means of studying the low latitude plasma. These emissions can be used as a way of remotely sensing the F region and exosphere properties, and the winds responsible for plasma transport.

CHAPTER 2

LITERATURE SURVEY

2.1 THE MODEL OF HARRIS AND PRIESTER

Harris and Priester[19] constructed a semiempirical model based on experimental data and the thermal balance problem of the thermosphere from 120 to 1200 km for various conditions of solar activity at selected local times. They defined the temperature dependace of a flowing ideal gas in an external gravity field as

$$\frac{\partial T}{\partial t} + \frac{\partial T}{\partial z} w + \frac{RT}{C_v} \frac{\partial w}{\partial z} = \frac{q}{C_v} \tag{2.1}$$

Where z is in vertical direction. Hence the change in entropy is due to the heat input. In above equation the w is vertical gas vlocity, q is the net gain of heat due to thermal sources (conduction, radiation), C_v is the specific heat at constant volume and R is the universal gas costant. In order to solve the above equation with standard mathematical method they assumed that:

$$T(z,t) = T_o(z) + T_1(z,t) \text{ and } T_1 \ll T_o$$

$$\frac{\partial T_1}{\partial t} + \frac{\partial T_o}{\partial z} w + \frac{RT_o}{C_v} \frac{\partial w}{\partial z} = \frac{q}{C_v} \tag{2.2}$$

If we consider a gas cell which moves vertically, at constant pressure with very slow motion, we have(to the first order)

$$P(z + w\Delta t, t + \Delta t) = P(z,t) \tag{2.3}$$

$$P_0 exp\left[- \int_0^{z+\Delta t} \frac{gm}{kT(t - \Delta t)} dz' \right] = P_0 exp\left[- \int_0^{z} \frac{gm}{kT(t)} dz' \right] \tag{2.4}$$

Expanding $(t + \Delta t)^{-1}$:

$$\frac{1}{T(t+\Delta t)} \approx \frac{1}{T(t)}\left[1 - \frac{1}{T(t)}\frac{\partial T}{\partial t}\Delta t\right] \tag{2.5}$$

substitute in equation (2.4) yields the following value for vertical velocity gradient:

$$\frac{\partial w}{\partial z} = \frac{\partial T_o}{\partial z}\int_0^z \frac{1}{T_o^2}\frac{\partial T_1}{\partial t}dz' + \frac{1}{T_o}\frac{\partial T_1}{\partial t} \tag{2.6}$$

substitute this form in equation (2.2):

$$\frac{\partial T_1}{\partial t} + \frac{\partial T_o}{\partial z}T_o\int_0^z \frac{1}{T_o^2}\frac{\partial T_1}{\partial t}dz' = \frac{q}{C_p} \tag{2.7}$$

which can be integrated numerically by considering the net gain of the energy due to

$$q = R_{cond} + R_{rad} + R_{EUV} + R' \tag{2.8}$$

where R_{cond} is the thermal conduction term

$$R_{cond} = \frac{\partial}{\partial z}k(T)\frac{\partial T}{\partial z} \tag{2.9}$$

$$k = \sum_i \frac{A_i n_i T^{\frac{1}{2}}(z)}{\sum_i n_i} \tag{2.10}$$

the symbols K, n_i, A_i refer, respectively, to the thermal conductivity, the number density of the ith constituent, and a constant varies from one constituent to another.

$$R_{rad} = -n(O)E_1A_{12}\left[\frac{W_1 exp^{\frac{-E_1}{kT}}}{W_2 + W_1 exp^{\frac{-E_1}{kT}} + W_o exp^{\frac{-E_o}{kT}}}\right] \tag{2.11}$$

where n(O)is the number density of atomic oxygen, E_0 and E_1 are, respectively, the energy differences between the $^3P_0$ and $^3P_1$ levels and between the $^3P_1$ and $^3P_2$ levels of atomic oxygen,W is the statistical weight of the level indicated by subscript, and A_{12} is the Einstein coefficent for transition $^3P_1$ to $^3P_2$. The R_{EUV}

term is the heat input due to solar EUV radiation obtained for multi component atmosphere and a continuous EUV spectrum,

$$R_{EUV} = \sum_i \epsilon_i n_i(z) \int_0^\infty d\lambda F_\lambda Q_i(\lambda) e^{-\tau_i(\lambda,z,t)} \tag{2.12}$$

$$\tau_i(\lambda, z, t) = Q_i(\lambda) \int_z^\infty \frac{n_i(z')dz'}{cos\chi(t)} \tag{2.13}$$

where $\tau_i(\lambda, z, t)$ is the optical thickness, F_λ is the radiation flux per unit wave length. ϵ_i is the thermal efficency, and $Q_i(\lambda)$ is the absorption cross section. Finally, R' is the heat source term representing other heating mechanisms, such as corpuscular radiation which is the energy radiated in the form of particles rather than electromagnetic waves. The boundary conditions are based on the empirical data. It shows that convegence of temperature happens if and only if the heat equation is integrated over a time span of several hours. They also found the number density profiles for each species. With the assumption that the atmosphere is in diffusive equilibrium above 120 km. By using the ideal gas law, and barometric equation, it can be proved that

$$n_i(z,t) = n_i(0)\frac{T(0)}{T(z,t)} exp\left[-\int_0^z \frac{m_i g(z')}{kT(z',t)} dz'\right] \tag{2.14}$$

Other properties such as molecular mass, scale height, pressure, mass density are then obtained from hydrostatic theory.Hydrostatic properties are approached through barometric equation which relates pressure gradient to the mass density.

2.2 LOW LATITUDE IONOSPHERIC MODEL

A technique described by many investigators in Hanscom Air Force Base labrotaries called low latitude ionospheric model. Anderson [3] solved the electron density as a function of latitude, altitude and local time by solving the time dependent ion (O^-)

continuity equation numerically. The effects of production by photoionization, loss through charge exchange with N_2 and O_2 and transport by diffusion, neutral winds and vertical $\overline{E} \times \overline{B}$ drift are included. Because $\overline{E} \times \overline{B}$ drifts play such an important role in determining the electron density distribution Hansom[17] Moffet[26] Anderson[3] and have a seasonal and solar cycle dependace Fejer[14], the calculations are carried out for equinox and solstice conditions for both solar cycle maximum and minimum periods.

The continuity equation is given by

$$\frac{\partial N_i}{\partial t} + \overline{\nabla} \cdot (N_i \overline{V}_i) = P_i - L_i \tag{2.15}$$

Where the N_i is the ion density, P_i is the ion production rate , L_i is the loss rate, and V_i is the ion transport property. In the ionosphere, plasma is transported along geomagnetic field lines by diffusion and by $\overline{E} \times \overline{B}$ drift Kendall [23] and Pickering [33]. Equation (2.15) is solved by transforming the independent spherical coordinates to a coordinate system parallei and perpendicular to $\overline{B}$.

Equation (2.15) can be written as

$$\frac{\partial N_i}{\partial t} + \overline{V}_{i_\perp} \cdot \overline{\nabla} N_i = P_i - L_i - \overline{\nabla} \cdot (N_i \overline{V}_{i_\parallel}) - N_i \overline{\nabla} \cdot V_{i_\perp} \tag{2.16}$$

Where $\overline{V}_{i_\perp}$ is given by $\frac{\overline{E} \times \overline{B}}{B^2}$ and $V_{i_\parallel}$ includes the effect of plasma diffusion and neuteal winds. The right hand side of the equation involves terms which are second order in coordinates parallei to $\overline{B}$. The left hand side is the time rate of change of plasma density in a frame of referance which drifts with the $\overline{E} \times \overline{B}$ drift velocity. Equation (2.16) solved numerically to give electron densities as a function of time, latitude, altitude. The set of models are used to solve continuity equation. Briefly the models are the following:

(A) The MSIS [28] neutral atmosphere model is used to calculate N_2, O_2, and O densities and the neutral temperature, as a function of altitude, latitude, local time and an F 10.7 cm flux of 180 units to represent the solar cycle maximum period.

(B) Production and diffusion rates are 5.5×10^7 for solar cycle maximum and 2.3×10^7 HZ for solar cycle minimum. The loss rate adopted from Torr[39] at top of the atmosphere.

(C) Plasma temperatures were chosen by IRI [21] model . Fiqure 2.1 illustrates the temperature ratio behavior for sunspot maximum Equinox season.

(D) The vertical $\overline{E} \times \overline{B}$ drift velocity observed by Woodman [42] is essential in producing the electron density distribution observed near the magnetic Equator. Adoption of six vertical drift model to represent, three seasons and solar cycle maximum. The different drift patterns are based on the Jicamarca incoherent scatter radar observations by Fejer [14]. Fiqure 2.2 displays the diurnal variations in drift for the Equinox season, solar cycle maximum.

(E) The geomagnetic field is represented by a dipole model whose axis is aligned with the earth's rotational axis with incorporation $\overline{E} \times \overline{B}$ drift models appropriate to the American sector and tilted dipole geomagnetic field with declination specified over the sensitive regions.

(F) The analytic formulation for the meridional neutral wind field is adopted which makes use of observations and theory. It is constructed on the basis of observed diurnal, semidiurnal, terdional, harmonic with latitude variations of amplitude and phase obtained from data by Forbes [15]. The general latitudinal pattern assumed is guided by the tidal calculations and the zonal wind velocity by Roble [35]. Table 2.1 illustrates analytic wind equations. The solsticial modifications to the mean and diurnal components adequately account for the main features of the observed seasonal and latitudinal dependace of the meridional wind . Fiqure 2.3 gives contour

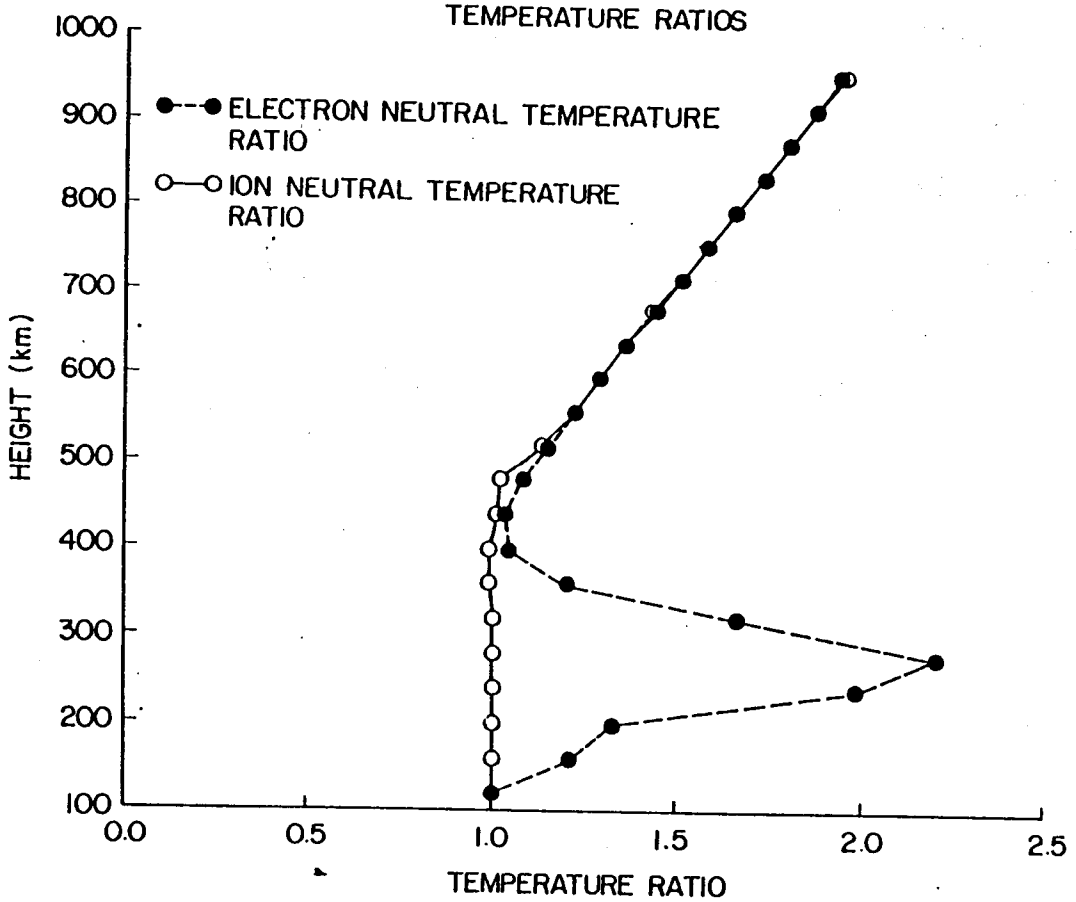


Figure 2.1 Ion-neutral and Electron-neutral Temperature Ratios as a Function of Altitude.

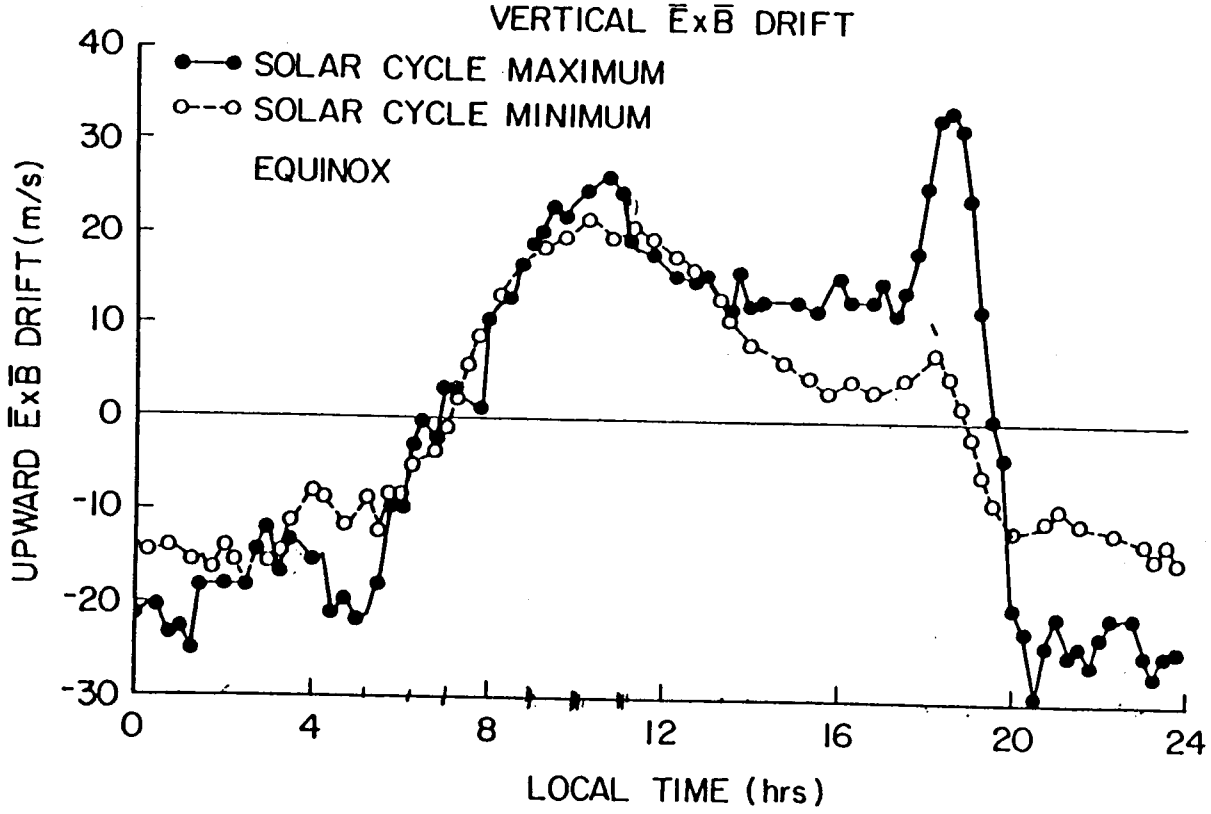


Fig 2.2 Upward $\overline{E} \times \overline{B}$ Drift Velocity Versus Time At Equinox Season.

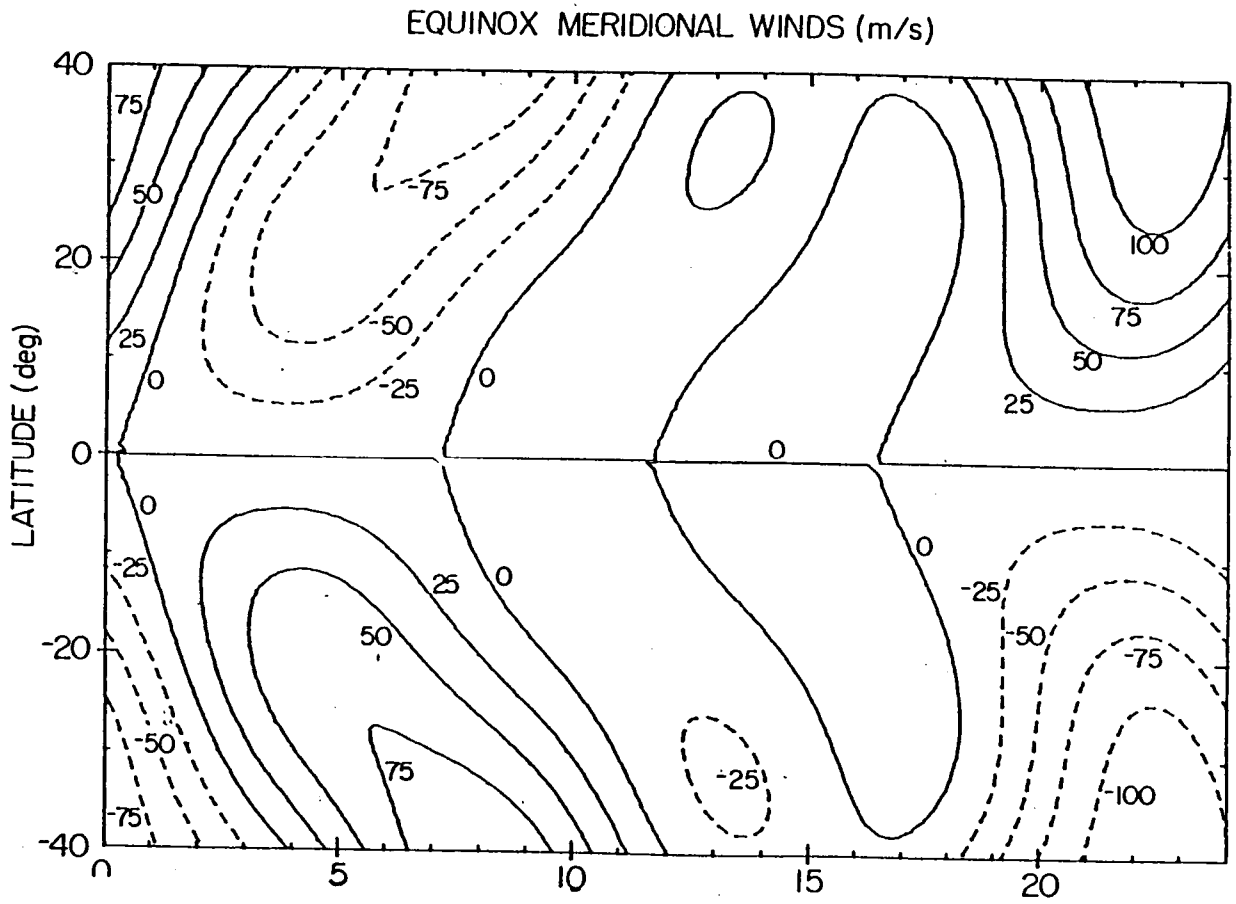


Fig 2.3 Contour Plots Of Meridional Winds Versus Latitude At Equinox Season.

Table 2.1 Analytic Wind Equations

Equinox

θ is latitude in degrees

$$V_0 = 8.61 \times 10^{-3} * \theta^2 \frac{\theta}{|\theta|}$$

$$V_{24} = 2\theta \cos \frac{2\pi}{24} (t - 18 - \frac{|\theta|}{7})$$

$$V_{12} = 50 \sin (\frac{\pi}{180} * \frac{10}{3} \theta) \cos \frac{2\pi}{12} (t - 9 - \frac{|\theta|}{12})$$

$$V_8 = 0.38 \theta \cos \frac{2\pi}{8} (t - 8.2 + 0.079 |\theta|)$$

$$V_{TOT} = V_0 + V_{24} + V_{12} + V_8$$

where

$V_{TOT} = V_0 + V_{24} + V_{12} + V_8$ (m/sec)

t = hours, local time

θ = geographic latitude, positive northern hemisphere

plots of the overall wind model spanning the simulation region.It is important to note while EUV varies markedly over a solar cycle, the associated variations in ion drag suppress solar cycle variations in the tidal winds, although neutral temperatures vary considerablly.Therefore, the model assumed the current wind parameterization to be independant of solar activity.

2.3 EMISSION OF OXYGEN AT 6300 Å

The post sunset is the result of excitation of atmospheric constituents by solar radiation, and to a smaller extent, by low energy electrons. Observations, however, are difficult because of the intense background of bright sky and solar Fraunhofer spectra. In order to observe post sunset from the ground, very high resolution and carefull analysis is neccessary. Successfull observations were made by resonance scattering of sodium, and results have been reported. The results can be used to design oxygen sensors, spectrometer, and photometer.

The OI nightglow is known to be produced almost by dissociative recombination of 0_2^+ and possibly NO^+. Zipf [43] studied the dissociative recombination of O_2^+ in the laboratory and found that branching ratio per production of (^3P)-(^1D)-(^1S) oxygen atoms at 300^oK to be 1.0, 0.9, 0.1, respectively(not inclding cascating effect). Quenching of $O(^1S)$ undergoes radiative transition to ^1D with the emission at the $5557\mathring{A}$ Forbes[15]. The theory of the $O(^1D)$ emission shows that the oxygen $O(^1D)$produced during the night time by the dissociative recombination of O_2^+, which can be proceeded by any of four processes:

$$O_2^+ - e \rightarrow O(^3P) + O(^3P) \tag{2.17}$$

$$O_2^+ - e \rightarrow O(^3P) - O(^1D) \tag{2.18}$$

$$O_2^+ + e \rightarrow O(^1D) + O(^1D) \tag{2.19}$$

$$O_2^+ + e \rightarrow O(^1D) + 0(^1S) \tag{2.20}$$

gives rise to the red line emission

$$O(^1D) \rightarrow O(^3P) \tag{2.21}$$

There is some doubt as to which of the following reactions results from the dissociative recombination of NO^+:

$$NO^+ + e \rightarrow N(^4S) + O(^1D) \tag{2.22}$$

$$NO^+ + e \rightarrow N(^2D) + O(^3P) \tag{2.23}$$

Peterson [32] suggested the possibility of $O(^1D)$ formation by quenching of $N(^2D)$ by $O(^3P)$. It was known that the relative contribution to the airglow intensity of the dissociative recombination of NO^+, as opposed to the dissociative recombination of O_2^+, is approximetly 10 percent. That implies 10 percent of the total 6300$\mathring{A}$ emission rate.Therefore, dissociative recombination of NO^+has significant contribution to the total 6300$\mathring{A}$ emission rate. It is important to emphasize that the exospheric temperatures for the data range from 800-1200 ^oK changes the number of excitation of $O(^1D)$ per recombination of O_2^+ including the cascading effect. The collisional quenching of $O(^1D)$ is important up to 300 km $O(^1S)$, on the contrary, doesnot suffer this fate except below 120 km. $N(^2D)$ is formed by dissociative recombination of NO^+; the state is quenched at all altitudes up to at least 550km by electrons and below about 250 km by O_2. The latest computed values for electron quenching of $N(^2D)$ suggest that this process dominates the loss rate in the F region above 250 km(F_2 region). Above 200 km the dominant ion is $O^+$and the rate of production

of the metastable is governed by the slower first step, the reaction of O^+ with O_2 or N_2.

2.4 EMISSIONS OF OXYGEN AT 7774Å ,1356Å AND 911Å

There are two mechanisms involved in producing oxygen 7774Å and 1356Å. one due to radiative recombination and the other due to ion-ion recombination. The prediction of radiative recombination as one of the F region recombination processes has been recognized and has been shown by Appleton[4] and Bates[5] and Dalgarno [12]. Radiative recombination is the process

$$O^+ + e^- \rightarrow O^* + hv' \tag{2.24}$$

where O^* is an excited state of neutral, and hv' is a photon of radiation which carries away the differance between the recombination energy and that of the excited or ground state of the neutral. Because of the Boltzman distribution of energies of the electrons, the recombination radiation hv' is in the form of continuum. Following the radiative recombination the excited atom decays to the ground state in a cascade transition of

$$O^* \rightarrow O + \sum hv \tag{2.25}$$

Radiative recombination results in one material body, in contrast to dissociative recombination, which results in two material particles. Thus it is more difficult to satisfy the need to conserve energy and momentum in radiative recombination than in dissociative recombination. The rate coefficents for radiative recombination is about five times smaller than for dissociative recombination as Vanzandt, and Tinsley [40] proved.

Ion-Ion recombination of oxygen is discussed by Knudsen [24] and Hanson [17]. It appears that Ion-Ion recombination contribute substantially to the observed tropical

UV airglow. For Ion-Ion recombination the negative ions are formed through the radiative attachment reaction

$$O + e \rightarrow O^- + hv \tag{2.26}$$

where hv is a continuum photon ($\lambda < 8463\mathring{A}$). It is clear by sattelite measuremants that the reaction must occur predominately at F_1 region. Some of the negative ions are lost through the associative detachment:

$$O^- + O \longrightarrow O_2 + e^- \tag{2.27}$$

and the remainder recombine in Ion-Ion neutralization

$$O^- + O^+ \rightarrow O^* + O^* + KE \tag{2.28}$$

leaving one or both oxygen atoms in an excited state, which can then decay or cascade to ground state in one or two transitions. Because only 12.149 ev is available for produced excited atoms, the possible transitions are fewer than those with radiative recombination.

The ionization potential of the oxygen atom is 13.61 ev which corresponds to a photon wavelength of $912\mathring{A}$. Solar photons of energy greater than this are available in the altitudes of the F and exospheric regions to produce O^+. The OI $911\mathring{A}$ is direct radiative recombination into the ground state.

2.5 PERTUBATIONS IN RADIO SIGNALS

Ionospheric disturbances caused by pulses of electromagnetic radiation are observed in the propagation of radio signals . Specific events affecting particular aspects of radio propagations in recent years are known as:

(A) Short Wave Fadeout(SWF)happens at frequency above 500 kHz in ionosphere and large flares can blackout the long distance short wave radio communications.

(B) Sudden Cosmic Noise Absorption is high frequency signals of extraterrestial origin which attenuated by atmosperic irrequlority and flares principally in D and F region.

(C) Sudden Enhancement of Atmospherics are reflections of low frequency phenomena in D region.

(D) Sudden Phase Anomaly is amplitude changes in phase of low frequency radio waves because of the electron concentrations in D and E region.

(E) Sudden Frequency Deviation observed on high frequency radio signals. Increased ionization in the E and F regions result in changes of refractive index of those regions for radio waves propagated through them. As the refractive index changes, so does the phase path, and this results in a change of frequency proportional to the rate of change of the ionization. Hence, the more impulsive the event, the more pronounced the Sudden Frequency Deviations.

CHAPTER 3

ANALYTICAL APPROACH

3.1 CHAPMAN FUNCTION

The hydrostatic properties of the upper atmosphere are conveniently approaced from the barometric equation which relates the pressure gradient to the mass density as

$$\frac{dp}{dh} = -\rho g \tag{3.1}$$

where the density can, in turn, be expressed in terms of the particle masses and number density of the various components as

$$\rho = \sum m_i n_i \tag{3.2}$$

Because of the very long mean free paths of the neutral particles at high altitudes, one can treat the gases as ideal. Dividing the equation (3.1) by the equation of an ideal gas

$$p = nKT \tag{3.3}$$

yields

$$\frac{dp}{p} = -\frac{\rho g}{nKT} dh \tag{3.4}$$

Where n is the total particle number density, T is the absolute temperature, K is the Boltzman constant, and m = $\frac{\rho}{n}$ is the average particle mass.

The quantity H = $\frac{KT}{mg}$ is referred to as the scale height, the distance in which the pressure of an isothermal atmosphere of constant composition drops by a factor

e^{-1}. The scale height is not constant and the integration of Equ (3.4) must be performed numerically.

Within a short range of altitude, however, it is always a good approximation to express the scale height as a linear function of altitude.

$$H = H_0 + \alpha h \tag{3.5}$$

Inserting this form of H into equation (3.4) and integrating,

$$p = p_0(1 + \frac{\alpha}{H_0}h)^{-\frac{1}{\alpha}} \tag{3.6}$$

and

$$n = n_0(1 + \frac{\alpha}{H_0}h)^{-(1+\frac{1}{\alpha})} \tag{3.7}$$

If one take the limit$\alpha \to 0$,

$$p = p_0 exp(-\frac{h}{H}) \tag{3.8}$$

as one expect for an isothermal atmosphere.

In any case, one can write the following equation for energy input:

$$q_T(h) = \sum_i \int F_\lambda(\lambda, h)\epsilon Q_i(\lambda)n_i(h)d\lambda \tag{3.9}$$

where $F_\lambda(\lambda, h)$ is spectral irradiance which is the radiation flux per unit wavelength of photons at height h, n_i is the number density of the ith species at height h, $Q_i(\lambda)$ is the absorption cross section, and ϵ_i is the amount of thermal energy liberated per unit radiation absorbed(thermal efficiency). Spectral irradiance can be obtained by the relation

$$F_\lambda(\lambda, h) = F_\lambda(\lambda, \infty)e^{-\tau(\lambda,h)} \tag{3.10}$$

$$\tau = sec\chi Q\int_h^\infty n(h')dh' \tag{3.11}$$

For monochromatic radiation of wavelength λ_0 and a single component exponential atmosphere by using equation (3.9)and (3.11) one can obtain,

$$q_T(h) = F(\lambda_0, \infty)n(h_0)\epsilon Q exp\left[-\frac{h}{H} - n(h_0)\sec\ \chi Q H exp(-\frac{h}{H})\right] \tag{3.12}$$

where h_0 is the zero point for altitude measurements. It is obvious that q should show a maximum at some height due to combined effects of increased heating rate and increased absorption rate of radiation with descending altitude . Eventually an altitude is reached where the attenuative effects in the atmosphere above offset the effect of higher local atmospheric density. One can easily determine this height by diffrentiating q(h) and equating to zero . The altitude of maximum absorption h_m is related to the other parameters by

$$h_m = Hln[n(h_0)QHsec\chi] \tag{3.13}$$

Inserting this result into equation (3.12) yields

$$q(h) = q(h_m)exp\left[1 - \frac{h - h_m}{H} - e^{-\frac{h-h_m}{H}}\right] \tag{3.14}$$

where

$$q(h_m) = \frac{F(\lambda_0)\epsilon cos\chi}{eH} \tag{3.15}$$

The above result is called the Chapman[11] function.

CHAPTER 4

GENERAL ANALYSIS

4.1 CHEMICAL RATE ANALYSIS TECHNIQUE

The ionic species formed initially in the F_2 region are the same as at the lower altitude, O^+, N_2^+, and O_2^+. Of these, the first two are important. The molecule ions can recombine directly via the usual dissociative processes,

$$e + N_2^+ \rightarrow N + N \tag{4.1}$$

$$e + O_2^+ \rightarrow O - O \tag{4.2}$$

which occur rapidly because of the large recombination coefficents. Atomic oxygen is a differnt case. The mechanism of direct recombination is neccessary radiative and is very slow. A more rapid means of electron removal is offered by the chain of processes,

$$O^+ + N_2 \rightarrow NO^+ + N \tag{4.3}$$

$$O^+ + O_2 \rightarrow O_2^+ + O \tag{4.4}$$

$$NO^+ + e \rightarrow N + O \tag{4.5}$$

The pertinent rate coefficents are ,

$$q(O^+) = (k_3[N_2] + k_4[O_2])[O^+] \tag{4.6}$$

$$\alpha_2[O_2^+]N = k_4[O_2][O^+] \tag{4.7}$$

$$\alpha_5[NO^+]N = k_3[N_2][O^-] \tag{4.8}$$

$$N = [O^+] + [NO+] + [O_2^+] \tag{4.9}$$

where N is the total ion number density, $q(O^+)$ is the inergy input for ionization process, and α and k rate coefficents. By eliminating $[O^+]$and $[NO^+]$ from equation (4.9) with the aid of equations (4.8)and(4.7), one obtain a relation between energy input and the total ion density

$$q(O^+) = \left(\frac{(k_3[N_2] + k_3[O_2])N}{1 + \frac{k_4[O_2]}{\alpha_2 N} + \frac{k_5[N_2]}{\alpha_5 N}} \right) \tag{4.10}$$

The rate constants corresponding to reactions (4.3)and(4.4)are, respectively, about 2 to $4.5 \times 10^{-12}$and 2 to 4.3×10^{-11} $cm^3 sec^{-1}$. For typical values of α_2 and α_5(1. 2×10^{-7}), and ion number density about 10^6 one can observe that

$$\left(\frac{k_4[O_2]}{\alpha_2} + \frac{k_3[N_2]}{\alpha_5} \right) \frac{1}{N} \ll 1 \tag{4.11}$$

if one considers the fact that the gain of O^+ is proportional to the gain of electron number density then,

$$\beta N = q(O^+) \tag{4.12}$$

at altitudes above 250 km , one obtain

$$\beta \approx k_3[N_2] + K_4[O_2] \tag{4.13}$$

where $[O_2]$=0.1 $[N_2]$ for 180 to 400 km, (Zipf[43]). BecauseN_2, O_2 have nearly the same scale height , therefore, they behave almost exponentially in an isothermal atmosphere.

4.2 THE SEMI EMPIRICAL IONOSPERIC APPROACH

The purpose of semi empirical ionospheric model technique is to identify a simple $N_e(h)$function that will have a small number of coefficents and yet provide a good representation of the profiles calculated from the theoretical model. The Chapman equation developed in chapter 3 is modified to produce the topside and bottemside components of the electron density profiles for solar cycle maximum at equinox season.

Modified Chapman function is defined as

$$N_e(h) = N_{max} exp\left[c(1 - Z - e^Z)\right] \tag{4.14}$$

where

$$Z = \frac{h - h_{max}}{A} \tag{4.15}$$

Six parameters are needed to produce the overall electron density profiles $(N_e(h))$, they are N_{max}, h_{max}, A_{up}, A_{lo}, C_{up}, C_{lo}.

There are three ways to produce electron density profiles.

1. Empirical model of CCIR[9].
2. Observed values by FY84 sattelite data[2].
3. Low Latitude Ionospheric Model by Hanscom Airforce Laboratory[3].

In our investigation $N_{max}, and h_{max}$ are provided internally by low latitude ionospheric model as discussed in chapter 2. Combination of C and A are tested until the sum of the square of the differences between modified Chapman function and Low Latitude Ionospheric Model is minimized.

$$\sigma(C, A) = \sum_{i=1}^{n} \left\{N_e^{Chap}(C, A, h_i) - N_e^{LLIM}(h_i)\right\}^2 \tag{4.16}$$

The range of values C and A in the loop are $C = \frac{1}{16} \longrightarrow 2.0$, $\Delta C = \frac{1}{16}$, $A = 10 \longrightarrow 200km$,$\Delta A = 10km$. Figure 4.1 shows a comparison between the modified Chapman function and Low Latitude Ionospheric Model.

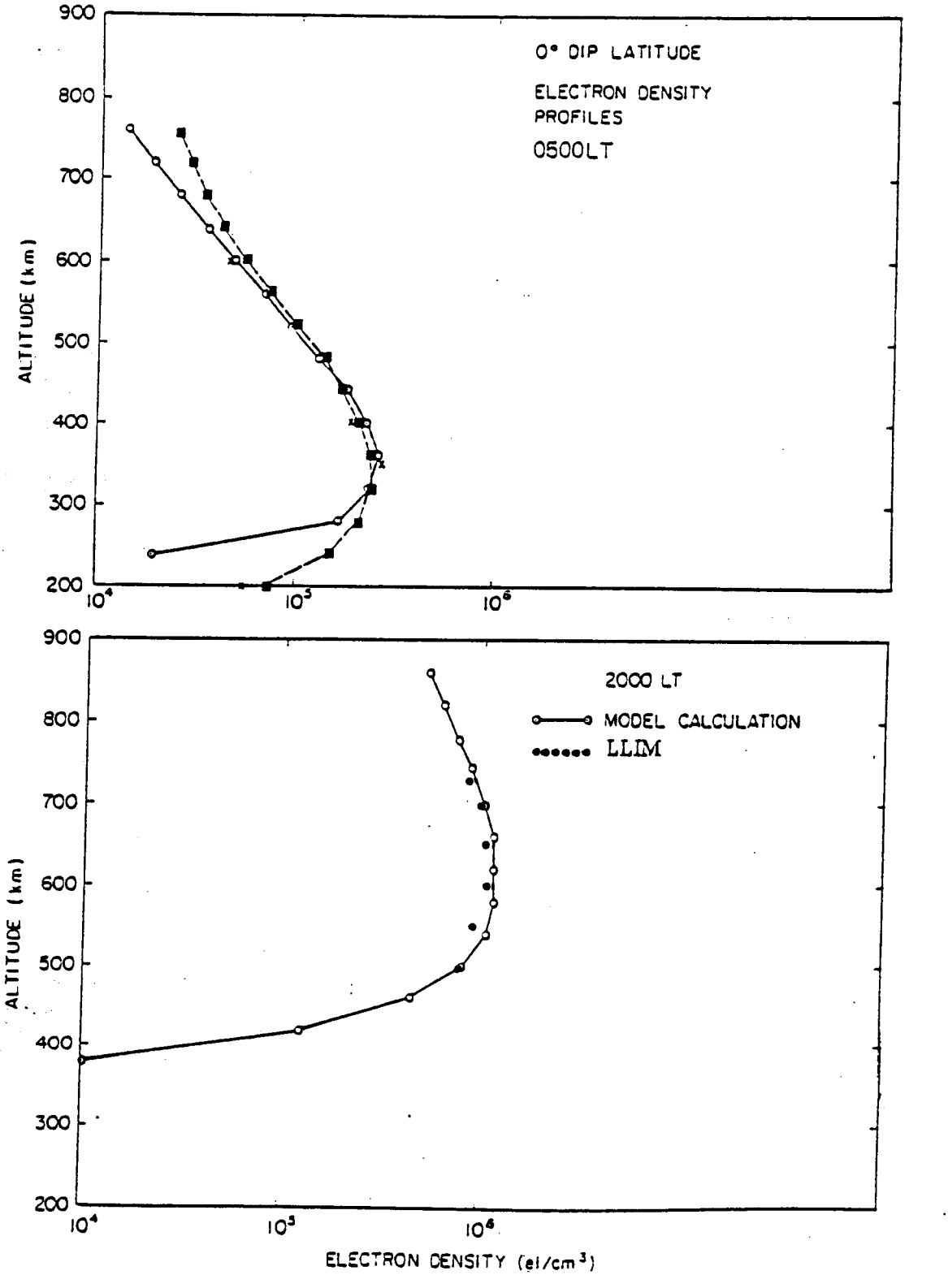


Fig 4.1 A Comparison Between The Modified Chapman Model and Low Latitude Ionospheric Model (LLIM) At 0500 LT and 2000 LT.

The total electron content calculated by integrating the profiles generated by modified Chapman equation for F_1, F_2, and exosphere plasma up to 1800 km. The above analysis carried out from 26S to 26N of geomagnetic latitude, for 24 hours, Equinox season, solar cycle maximum.

4.3 VOLUME AND COLUMN EMISSION RATE OF OXYGEN

Based on the modified Chapman function density profiles,the column emission rate at 6300Åairglow intensity using the following formula calculated.

$$R_{Rayleigh} = \frac{A_{6300}}{10} \int_{180}^{1800} \left[\frac{K_1[O_2][e^-]}{A_{tot} + K_2[N_2] + K_3[e^-] + (K_4)[O_2]} \right] dh \qquad (4.17)$$

where

$$K_1 = 2 \times 10^{-11} \left(\frac{300}{T_n} \right)^{\frac{1}{2}}$$

$$K_2 = 2.3 \times 10^{-11}$$

$$K_3 = 2 \times 10^{-9}$$

$$K_4 = 5.3 \times 10^{-11}$$

$$A_{tot} = 0.00681$$

$$A_{6300} = 0.00515$$

All the K values, A_{tot} and $A_{6300}$are in units of $\frac{cm^3}{sec}$, $\frac{1}{sec}$ and $\frac{1}{sec}$, respectively. The O_2 and N_2 concentrations has been obtained by MSIS[28] neutral atmosphere. The column emission rate of oxygen at 7774Å obtained by considering Ion-Ion recombination and radiative recombination.

$$I_{radiative} = \int \alpha V(h) dh \qquad (4.18)$$

where volume emission is defined as,

$$V(h) = n(O^+)n(e) \tag{4.19}$$

$$\alpha_{7774} = .75 \times .625[\alpha_t - \alpha_{gs} - \alpha_{3s}] \tag{4.20}$$

where α_t is the total coefficent, α_{gs} is the ground state coefficent, and α_{3s} is the direct recombination to the specified state. The Ion -Ion recombination intensity can be calculated by the relation,

$$I_{(Ion-Ion)} = \int \frac{\beta_i K_2 K_1 n(O)[n(e^-)]^2}{K_2 n(e^-) + K_3 n(O)} dh \tag{4.21}$$

$$K_1 = 1.3 \times 10^{-15}$$

$$K_2 = 1.5 \times 10^{-7}$$

$$K_3 = 1.4 \times 10^{-10}$$

$$\beta_{7774} = 0.42$$

the column emission rate of oxygen at 1356$\mathring{A}$ can be calculated by the same equations with different radiative and Ion-Ion rate coefficents. The rate coefficent by radiative recombination at 1200 ^oK is given by

$$\alpha_{1356} = 0.625\alpha_t - \alpha_{gs} \tag{4.22}$$

the rate coefficent for$\alpha_{1356} = 7.108 \times 10^{-13}$, $\alpha_{7774} = 5.1 \times 10^{-13}$, $\alpha_{911} = 3.23 \times 10^{-13}$. where α_{911} is direct recombination to the ground state.

CHAPTER 5

DISCUSSION OF RESULTS

5.1 ELECTRON CONTENT

Figure 5.1 shows the development of the anomaly at different magnetic latitudes during the equinox period, a time of sun spot maximum. The so called equatorial or Appleton anomaly manifests itself as an anomalous electron and ion distribution. Fig 5.1b shows the existance of two peaks in total electron content(TEC) .one on either side of the magnetic equator ± 16 degrees dip latitude. The maximum of TEC at equator is about 32 percent less than of 16 latitude. At equator, the decrease in TEC between 1800 and 2000 local time is precipitous during the solar cycle maximum period. This is due to large post sunset enhancement in upward $\overline{E} \times \overline{B}$ drift, which is a common feature at solar cycle maximum. In fact the sharp drop of TEC and N_{max} can be considered a sign that the F layer is rising rapidly after sunset and that the range type of incident vertical electromagnetic wave reflection is likely appearing (spread F). Spread F negatively correlates with magnetic activities. and maximum incidence occurs at equinox period as dicussed by Rastogi[41]. The low values of N_{max} and TEC at night is also due to the neutral winds which blows toward the equator causing a convergence of plasma there. The neutral winds move ions across magnetic field lines, thus loss rates become significant. In addition, at F region heights at night, thermospheric winds are capable of generating electrostatic fields which significantly affect ionospheric plasma electron density (Rishbeth [34]). Loss of ionization in a two step processes in which O^- charges exchanges with N_2 and O_2^+ which subsequently dissociatively recombine with electrons. The loss rate

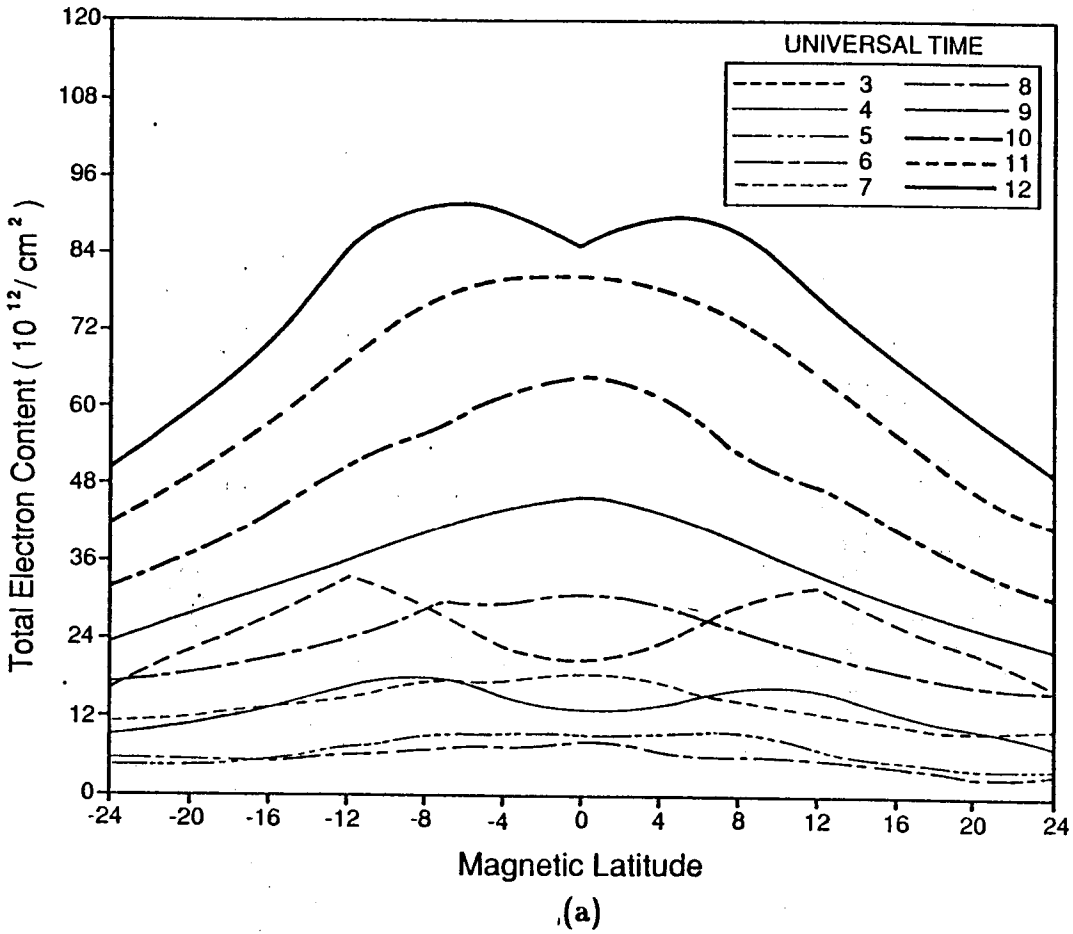
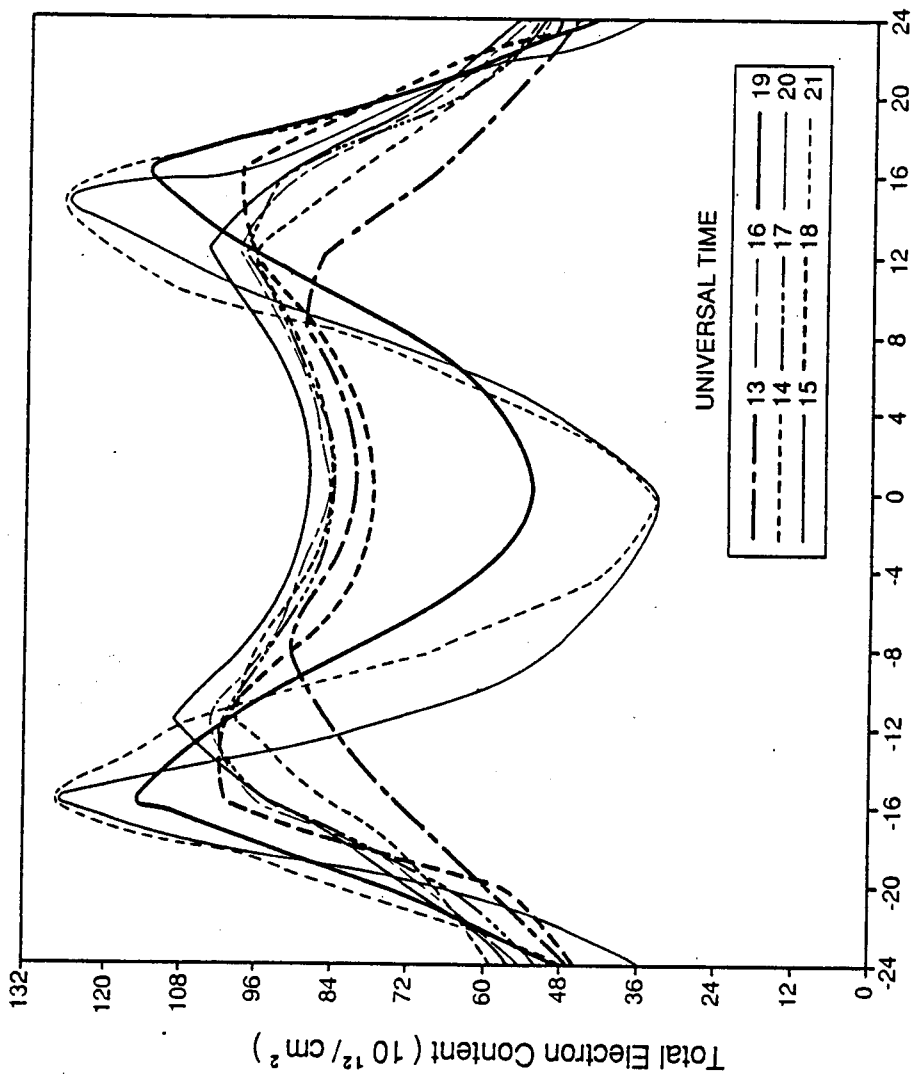
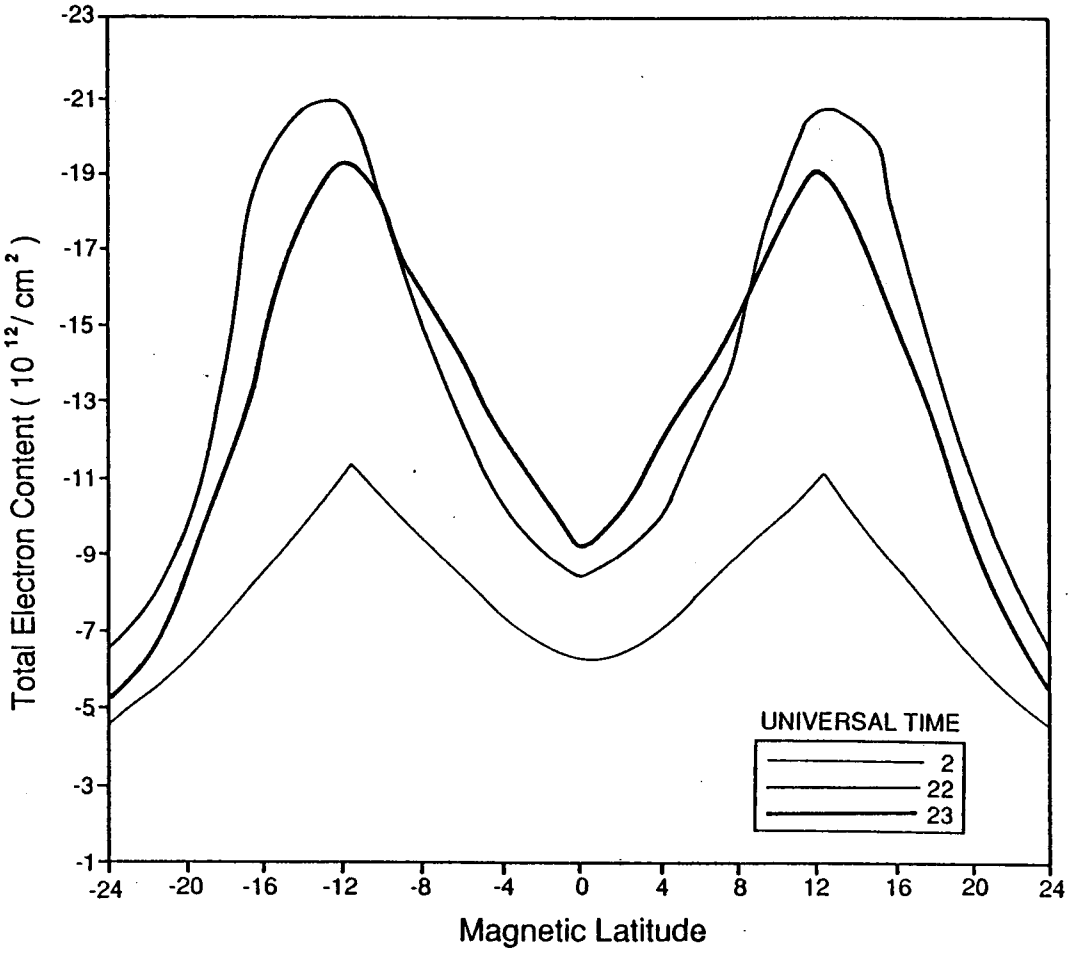


Fig 5.1 Total Electron Content Versus Magnetic Latitude For Sunspot Maximum At Equinox Season.



(b)

Fig 5.1 :Continue.



(c)

Fig 5.1 Continue.

decreases with increasing altitude so that transport processes become more and more important. Forces acting on the F region and exosphere plasma include the Earth's gravitational field , plasma pressure gradients, collisions between charged and neutral particles and electrostatic fields. Because of the presence of a magnetic field , however, charged particles cannot, in general, move in the direction of applied force. Since the ion cyclotron(gyro frequency) is much greater than the ion neutral collision frequency at F region altitudes, non electromagnetic forces such as gravity, pressure gradients and neutral winds, transport ionization along magnetic field lines while electromagnetic forces due to an electrostatic field, $\overline{E}$, effectively move plasma perpendicular to $\overline{B}$ (Moffet[26)]. This electrostatic field is produced initially in the ionospheric E region as a consequence of the neutral winds, ions move across magnetic field lines thereby generating currents which cause instability in ionpsphere. There is always a strong coupling between the plasma and the magnetic field which in fact, support a mode of wave propagation such as hydro magnetic mode. The exact character of the hydromagnetic wave is not known because of extreme complexity of the wave structure, but wave dissipation does lead to local heating of the plasma.

It is important to know that at equatorial latitudes the geomagnetic field lines are nearly horizontal in F_2 region.

Fig 5.1c, and 5.1a shows that the crests start moving equatoward from 0200 to 0600 local time,where the distribution becomes almost symmetric. The crests start forming again at 0700 and 0800 LT in south of the equator and they disappear at 0900 LT. It is important to notice, there is no crest in north of the equator at these times. They start forming again close to the equator around 1000LT, move poleward until 1900 LT, when the post sunset enhancement in upward $\overline{E} \times \overline{B}$ drift is a maximum. The peaks start moving back toward the equator at 2000LT. The

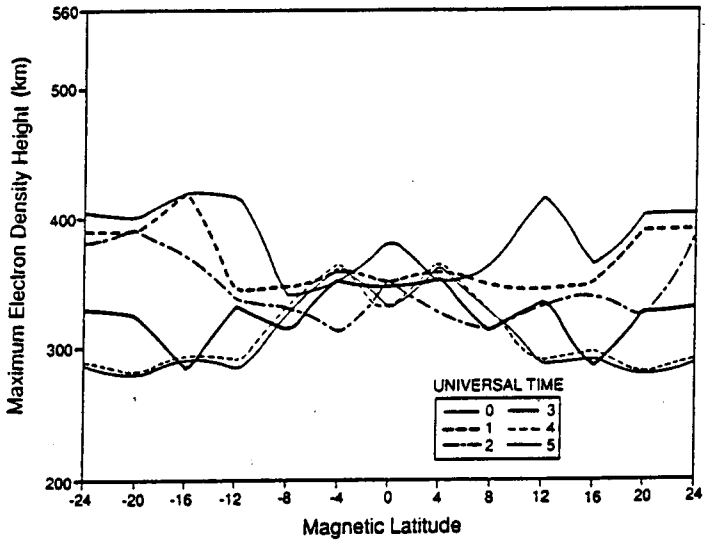
maximum TEC occurs at 2100 LT.

Fig 5.1b, and 5.1c indicates that during the solar cycle maximum period the anomaly reaches its maximum development around 2100 LT with the crest nearest the equator being the greatest. This asymmetry reverses by 0200LT with the crest farthest from the equator being the smallest. The above two statements define the equatorial and Appleton anomaly in a new fashion in terms of TEC.

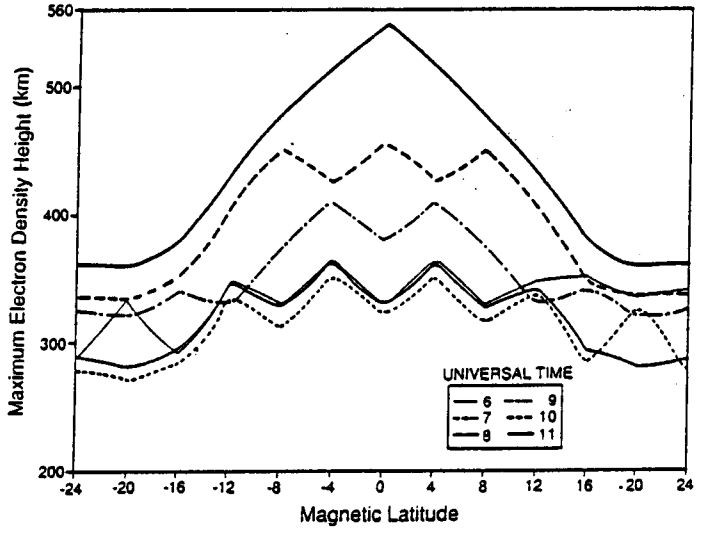
Fig 5.1a shows noon bite out for the magnetic equator occur in the total electron content except at 1000 LT and 1100 LT. This behavior is due to the fact, that the F layer becomes broader in altitude under the influence of upward drift so that no decrease in the content is observed. TEC starts increasing following the sun rise at the equatorial region and reaches its maximum at 1500LT, following the enhancement of $\overline{E} \times \overline{B}$ drift observed by Woodman[42].

The maximum electron density height versus magnetic latitude is shown in figure 5.2. The profiles of the peak electron density is a maximum at the equator following the day time enhancement of the $E \times B$ upward drift (Fig 5.2b). At the equator the maximum electron density height decreases following the depression of the maximum upward drift at night except at 0200 local time as shown in Figure 5.2a. Fig 5.2d shows the maximum electron density height happens to be at 1900 LT following the night enhancement of the $\overline{E} \times \overline{B}$ upward drift. As one can indicate, the electron density distribution and TEC is strongly influenced by vertical $\overline{E} \times \overline{B}$ drifts.

The $\overline{E} \times \overline{B}$ drift during daytime is predominantely upward. This upward drift, acting in combination with ambipolar diffusion and neutral wind transport the ionization away from the equator toward higher altitudes. As a result, the electron density and TEC near the equator decreases, and there is corresponding increase near 16 degrees latitude. The diurnal variation of the vertical $\overline{E} \times \overline{B}$ drift has

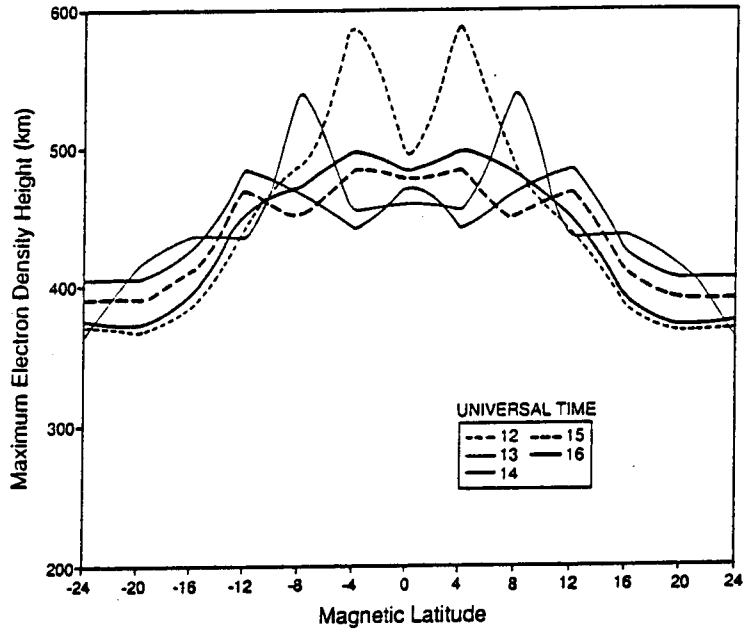


(a)

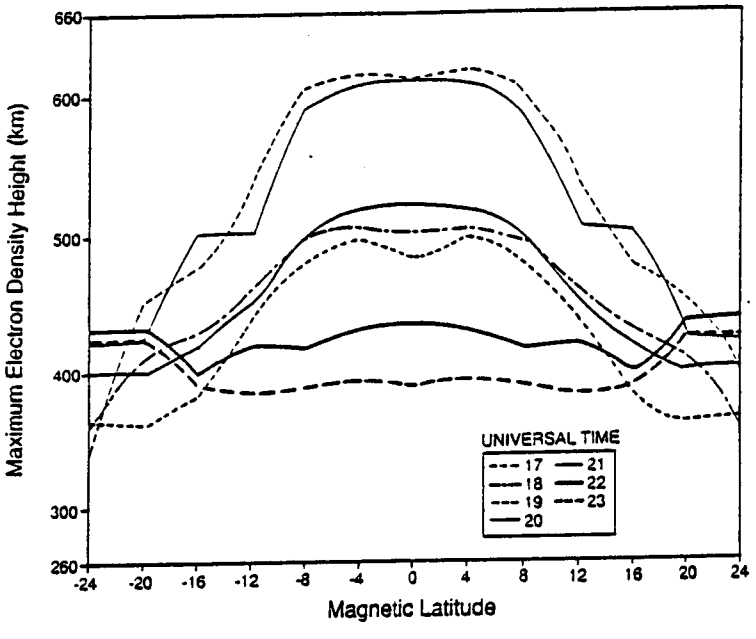


(b)

Fig 5.2 :Maximum Electron Density Height Versus Magnetic Latitude For Sunspot Maximum At Equinox Season.



(c)



(d)

Fig 5.2 Continue.

been measured, using the incoherent scatter radar facility at Jicamarca. These measurements show a general upward drift during the day and downward during the night. A common feature of the drift pattern is a sharp increase in the upward drift just after sunset but before the characteristic downward drift begins. After sunset the upward $\overline{E} \times \overline{B}$ drift raises the F layer region ionization to high altitudes, typically 550km later, the $\overline{E} \times \overline{B}$ drift is downward , and the ionization that earlier was raised to high altitudes is forced down to lower altitudes. Current empirical models of the low latitude ionospheric F region can servely underestimate the day time plasma total electron content when compared to actual observations. The most dramatic differences between our calculations and empirical models occur after sunset. At the magnetic equator, the post sunset enhancement in upward drift lifts the F layer to 610 km compared to h_{max} values of 500 km for the Harris and Priester[19] model and 450 km for Bent [6] model. Such differences in h_{max} would cause significant differances in the calculations of oxygen at 6300$\mathring{A}$ airglow intensity which is the brightest dayglow source, and the ion-neutral drag coefficent in the neutral momentum equation as discussed by Roble [35].

There are several factors that one need to consider in analyzing the F layer and exosphere plasma behaviors. One of the most important factor is the effect of the vertical$\overline{E} \times \overline{B}$ drifts on neutral winds. At F layer heights the ion drag acting on the neutral gas is proportional to the electron density. Therefore, a variation in the electron density results in a pertubation in neutal gas dynamics. The magnitude of the neutral atmosphere response depends upon the scale size of the electron density variations as dicussed by Dickenson [13]. The neutral gas accelarates shortly after sunset as the F layer is raised to high altitudes by$\overline{E} \times \overline{B}$ drift, and the ion drag acting on the neutral gas is reduced. Several hours later the neutral wind decelerates as the F layer is driven to lower altitudes by downward$\overline{E} \times \overline{B}$ drift, increasing the ion drag

on the neutral gas. The resuting divergence and convergence of the neutral winds give rise, to upward and downward vertical motions. The vertical motions cause adiabatic cooling and heating, therefore, it changes the rate of ionization. Thus the neutral gas temperature decreases at a more rapid post sunset decay rate due to the raising the F layer and exosphere plasma to high altitude by the $\overline{E} \times \overline{B}$ drift. Also, a neutral gas temperature increase would be expected near the midnight as the F layer is driven to the lower altitudes by the downward $\overline{E} \times \overline{B}$ drift. As one can notice, the above analysis ignored the effect of pressure forces acting on the neutral gas, and assumed the neutral gas motion is mainly controled by ion drag. However, an interaction will always occur, because the neutral wind is greater than the ion drift, and electron density change of about several order of magnitude occurs as the F layer descends. Since the upward drift of ionization after sunset and its subsequent reversal are a common occurance at the equator, one can deduce that F layer interaction with neutral gas occurs requlary.Before midnight the neutral wind is large because of reduced ion dag the F region moves to exospheric regions.As the layer descends, the increased ion drag causes the neutral wind to decrease. Through the continuity the convergence of the neutral wind results in downward vertical motion.The above analysis can be improved by Rishbeth's model [34] of the temporal variations of the upper ionosphere. He suggested that the neutral wind at night, which forces ionization perpendicular to the geomagnetic field lines, causes a polarization field to develop that in turn drives the F region and exosphere ionization in the direction of the neutral wind, therefore, the ion and neutral particle drag becomes smaller. Nevertheless,the phase of the local time variations of the wind component controls the shape of diurnal variations of the height and number density of the F_2 peak. The local time when the component changes from poleward to equatoward effects the preservation of the F_2 peak.

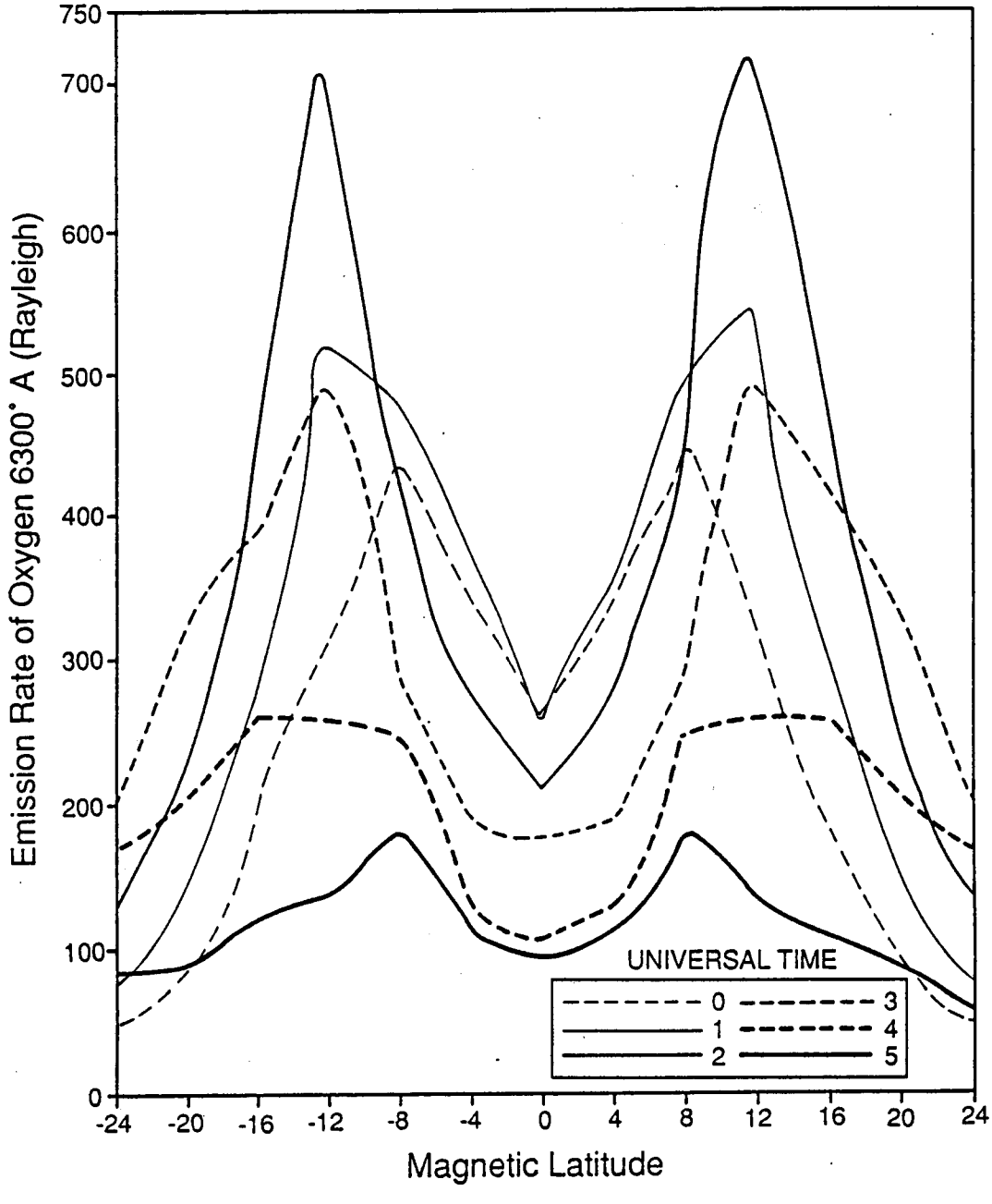
5.2 EMISSION RATE OF OXYGEN AT6300Å

The major ion found in the F_2 region and exosphere plasma is O^+ and its number density about equal the electron density.The ionization potential of oxygen atom is 13.61 ev which corresponds to a photon wavelength of 911Å.Solar photons of energy greater than this are readily available in the altitudes of the exosphere to produce O^+ by the reaction,

$$h\nu(912\text{Å}) + O \rightarrow (O^-) + e \tag{5.1}$$

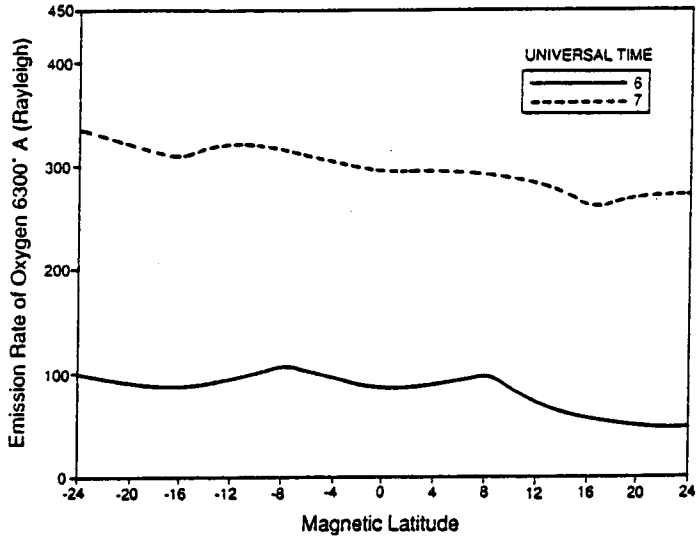
Measurements of the number density of O^+ in the Appleton anomaly by Chandra [10] from OGO-4 showed that dissociative recombination produces OI 6300Å emission, with emission rate varying both $N_{max}F_2$ and $h_{max}F_2$.

Figure 5.3 shows the column emission rate of oxygen at 6300Å versus magnetic latitude. Fig 5.3e, and 5.3f shows that the minimum of the emission rate occurs at night following the depression of $\overline{E} \times \overline{B}$ at equator. The maximum of column emission rate is $\pm 13^o$ at 0200 local time as shown in Figure 3a. The form of OI emission arcs is shown dramatically in far ultraviolet pictures of the earth obtained from the surface of the moon by Carruthers and Page[8].The apparent joining of the equatorial bands is believed to be the result of prospective, although some discussions continues regarding the proper interpretation of the picture. Figure 5.3e shows that the anomaly crests move from 20 degree at sunset to 8 degree at midnight on the average. Fig 5.3d shows that the minimum of the emission rate falls to 4 degrees latitude at 1700 local time. Measurements of ion density by the Bent[6], ion mass spectrometer on board the Atmosphere Explorer C Sattelite (AE-C), and by rocket-borne spectrometer, Goldberg [16] and Narcisi [29] indicates that after sunset near the magnetic equator, NO^+ and O_2^+ are dominant at lower altitude and O^+ is the dominant ion only at higher altitude. The observations imply that

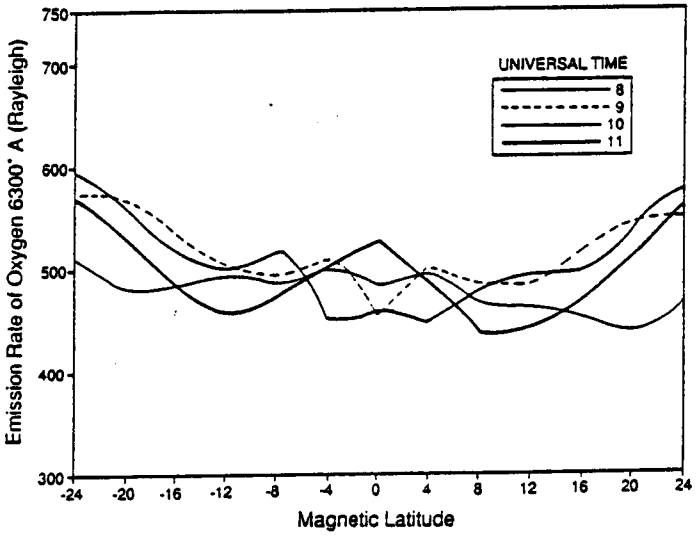


(a)

Fig 5.3 Column Emission Of Oxygen At 6300Å Versus Magnetic Latitude Sunspot Maximum At Equinox Season.

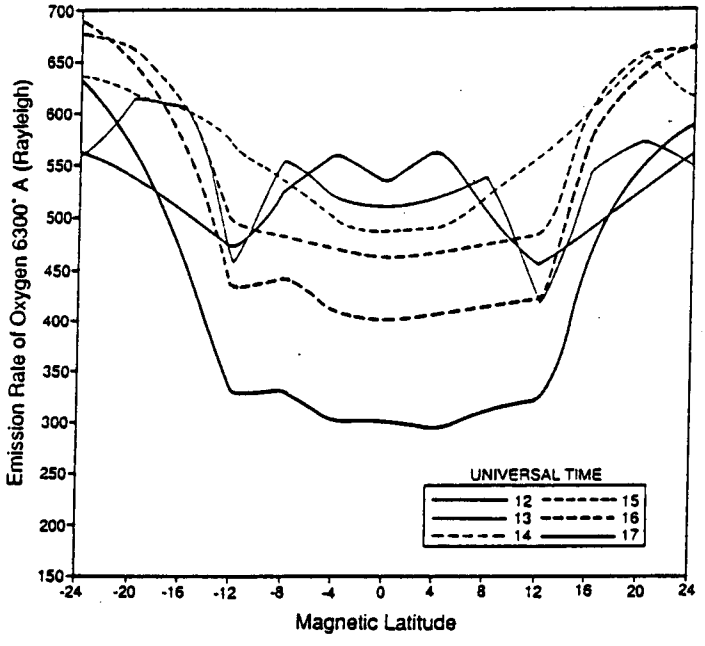


(b)

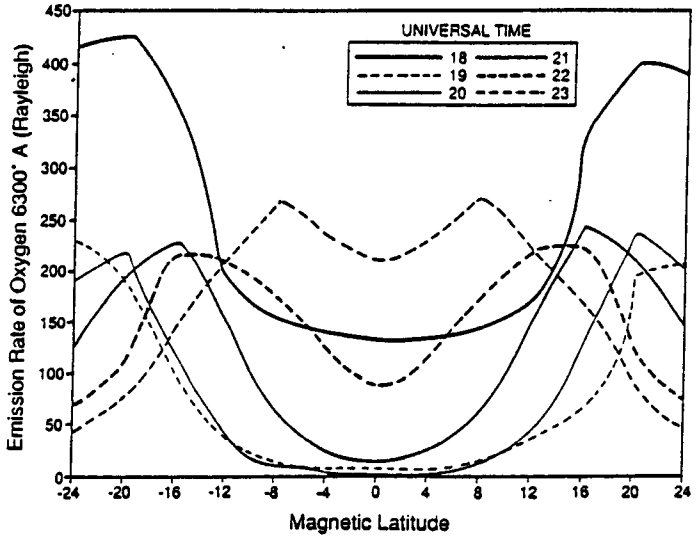


(c)

Fig 5.3 Continue.

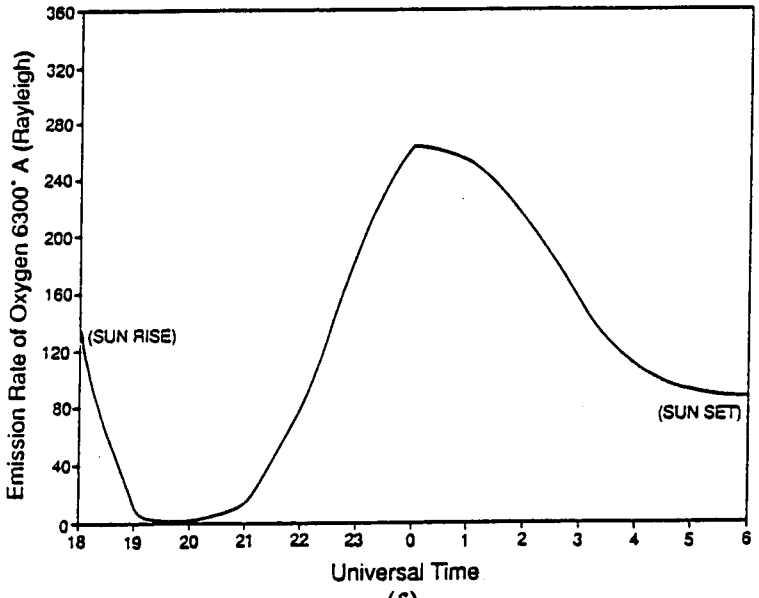


(d)

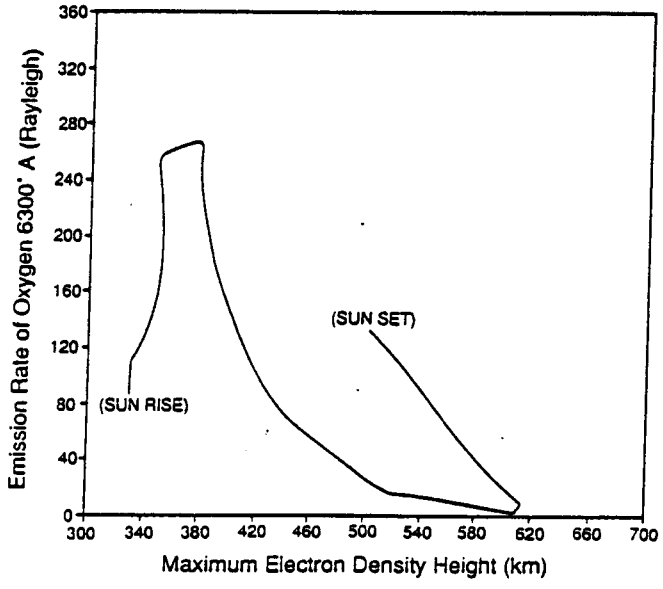


(e)

Fig 5.3 Continue.



(f)



(g)

Fig 5.3 continue.

upward transport is an important physical processes, which affects the molecular ion distribution and it also implies the importance of radiative recombination of NO^+, and the abundance of $O(^1D)$, which contributes significantly in the calculation of emission rates at 6300$\mathring{A}$ due to dissociative recombination.

Bittencourt and Sahai [36] studied the behavior of 6300$\mathring{A}$ emission at equatorial zone and found , that the emission at 6300$\mathring{A}$ enhancement is closely related to the time behavior of vertical $\overline{E} \times \overline{B}$ drift, its magnitude and time of reversal.They found;

1. When the post sunset enhancement in upward drift is well developed and downward drift commences after 2000, the maximum emission occurs around 0200 local time.

2. When upward drift is less and downward drift occurs at 1900 LT, the maximum 6300$\mathring{A}$ intensity occurs around 2300 LT.

Fig 5.3f justifies the above conclusion for the second case at the equator and contradicts the first case. As a matter of fact the data demonstrates that when the post sunset enhancement in upward drift is well developed, then the minimum 6300$\mathring{A}$ column emission rate occurs around 2000LT. Nevertheless, the first statement is correct for 13° geomagnetic latitude , and the second statement is contradicted for 13° geomagnetic latitude.

Fig 5.3g shows the maximum electron density height at equator versus the column emission rate at night. One observes that the minimum column emission rate corresponds to a peak of the maximum electron density height, at which altitude $O^+$is the dominant specie, whereas NO^+ and $O_2^+$are dominant in lower altitude. The data gives the value h_{max}=611 km, which is in the exospheric region. The radar measurements show that a significant portion of the emission comes from above the F peak, thereby making it difficult to perform precise calculations with the ionosonde data. Measurements of Oxygen at 6300$\mathring{A}$ showed that near magnetic

equator, just after sunset, the intensity drops to less than 10 Rayleighs due to the high altitude of the bottomside of the F layer. The above measurements correlate with our data at 2000 local time, when the post sunset enhancement of vertical $\overline{E} \times \overline{B}$ drift is well developed and downward drift commences after that.

Nightglow emission from the F region and exosphere plasma appears to be the result primarily of reactions involving charged particles.There are two factors need to be considered.

(a) The various reactions which remove O^+.

(b) Low energy electron excitation.

As one can expect, significant excitation of $O(^1D)$ occurs by low energy electrons in F region. Noxon [30] studied the behavior of low energy electrons when conductive heat flow from protonosphere leads to an appreciable rise in the electron and ambient temperature in the F region.The conjugate flux is thought to be responsible, at least in part, for the pre dawn enhancement of 6300$\mathring{A}$ which occurs at equinox well before the onset of local photoelectron production. It appears that the direct excitation of $O(^1D)$ is sensitive to local ionospheric conditions, in particular, upon the ratio $\frac{n(e)}{n(O)}$; when the latter is large a major fraction of conjugate photoelectron energy is deposited in the local elctron gas and less goes to O. Some of the pre dawn enhancement, at some locations, is a direct result of a lowering of the F layer and the consequent of ionic recombinations. Depending upon local conditions the enhancement due to direct excitation of O by conjugate photoelctrons may vary from 10 to 100 Rayleighs (Johnson [22]). One can observe how the low energy electrons are significant in calculating the OI 6300$\mathring{A}$.

In a rocket experiment (NASA 18.31 UA) launched from Wallops Island, Virginia, the emission rate at 6300$\mathring{A}$ were measured. Evaluation of the roles of electron impact excitation of the emissions led to the accurate description of the height

profiles of excitation for all of the relevant mechanisems. Specially the dissociative recombination of O_2^+ and the electron impact of atomic oxygen were found to be important at 6300$\AA$ (red line) and 5557$\AA$ (green line). The 6300$\AA$oxygen measurements of O_2^+ excitation due to dissociative recombination inferred from the data.Only small contributions from electron impact to the emission up to 240 km are apparent during sunrise. However, the photodissociation excitation of$O(^1D)$ and $O(^1S)$ atoms is evident from the measurements. The $O(^1S)$ doesnot have a significant contribution at F region.

Figure 5.4 shows the 6300$\AA$ volume emission rate of oxygen versus altitude.The 6300$\AA$ peak at O5OO LT, and O6OO LT doesnot change significantly and both profiles have significant emission rates at lower altitudes. At 0700 LT the volume emission rate peak goes up by a factor of 2 to 3 and volume emission rate at F_2 region increase significantly. At 0800 LT the volume emission rate peak increases but the plasma shifts to the lower altitudes. It is shown that at 0700 LT the F_1 region almost disappears and the distribution lifts the F_2 peak, but at 0800 LT the OI 6300$\AA$ becomes significant at F_1 region. This phenomena can be explained in terms of vertical $E \times B$drift such that the upward drift lifts the plasma at 0700 LT and depresses the region at 0800 LT(refer to Figure 2. in literature). The measuremeants of 6300$\AA$ emission rate between 100-240 km are about 50 percent for photodissociation , 13 percent for electron impact, and 37 percent for dissociative recombination. At 240 km and above the measurements show 15 percent for photodissociation, 47 percent for electron impact and 38 percent for dissociative recombination (Schaeffer, and Feldman [37]). The collisions of low energy electrons with atoms and molecules are important for several reasons. First. They control the cooling rate of the electron gas in regions where the neutral particle density is much greater than the ion number density.

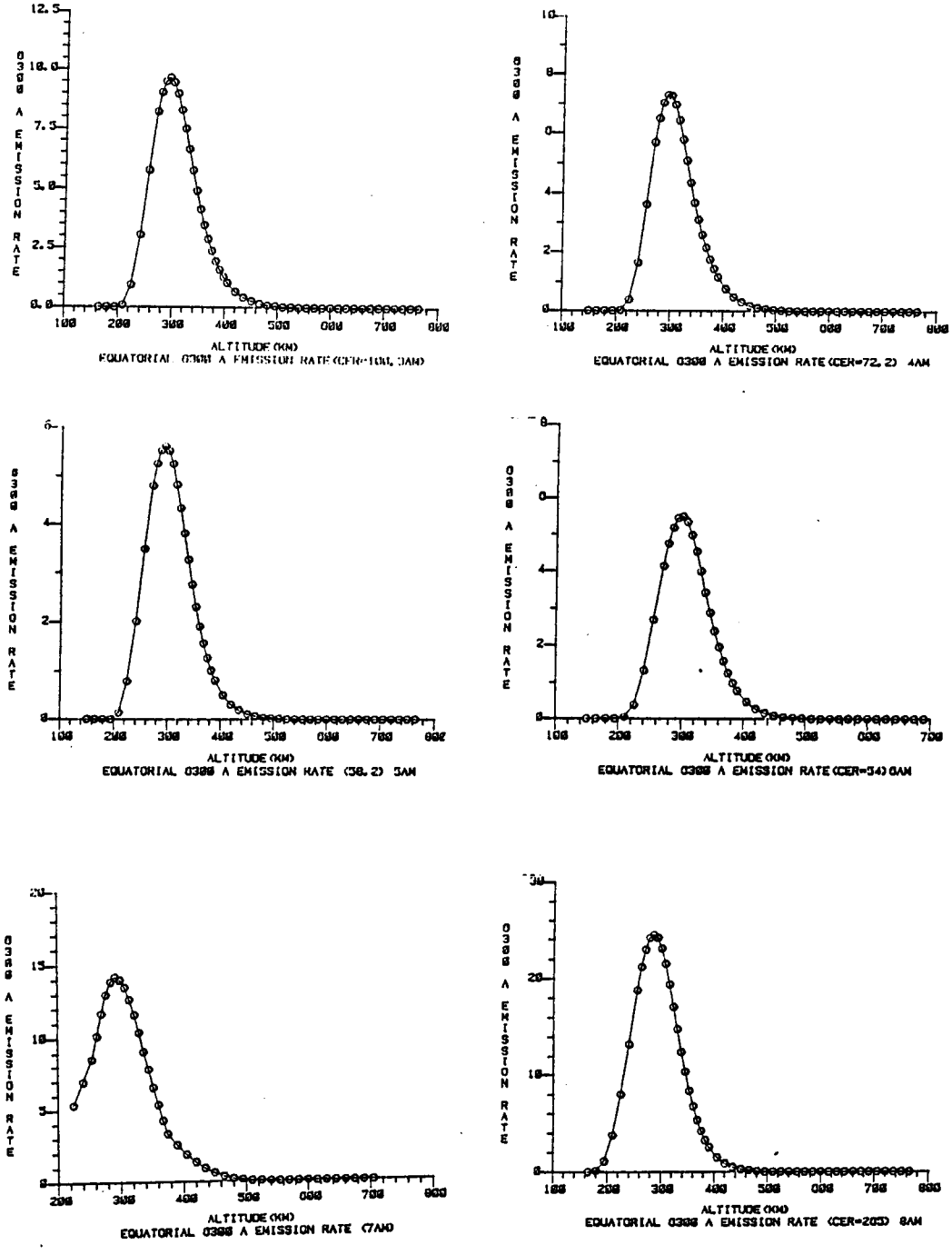
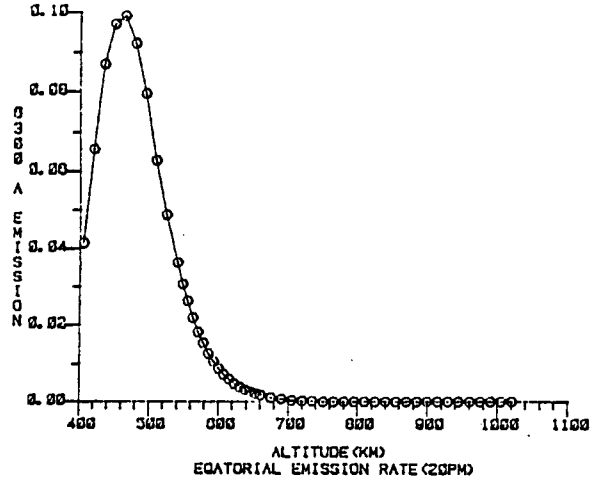
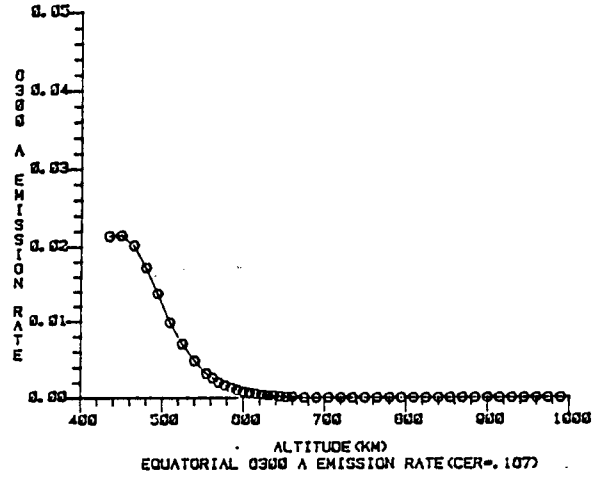
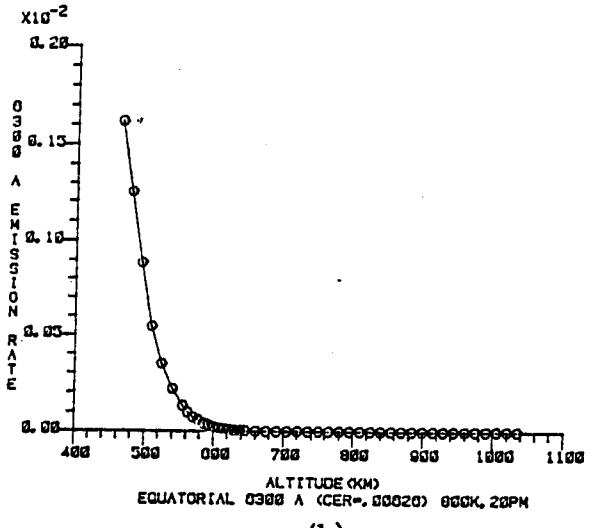


Fig 5.4 Equatorial Volume Emission Rate Of Oxygen At 6300Å Versus Altitude For Sunspot Maximum At Equinox Season.







(b)

Fig 5.4 Continued.

Secondly, they control the rate at which the ambient electron gas in an ionosphere extracts energy from the electromagnetic wave and hydromagnetic wave in the radio frequency range and transform it into the kinetic energy of random molecular motion. Thirdly, the vibrational modes of ground state nitrogen and oxygen molecules are quite excited by impact of electrons.

Figure 5.4b show that at 2000 LT, the volume emission rate peak drop by a factor of 4.5 from 1200 to $1000^{o}K$ and volume emission rate peak drop by a factor of 60 from 1200 to $800^{o}K$ at the equator. The results correlates with Peterson [32] investigations. He explained that the exospheric temperatures for data range from 800-1200^{o}K changes the number of excitation of $O(^{1}D)$per recombination of O_2^+ (including the cascading effect),therefore, the emission rate changes significantly.

The above investigations not only provide a basis for understanding the nature of the equatorial airglow but also provide useful means for estimating ionospheric parameters. The cause for the asymmetry in the height of the F_2 peak is also the vertical movement associated with the neutral wind,Rishbeth [34]. A meridional wind blowing from south to north of the geomagnetic equator tend to move the ionization upward to the south of the geomagnetic equator and downward to the north, Abur-Robb and Windle [1]. In this situation the F_2 peak will be higher south of the equator resulting in the asymmetric distribution in the airglow emission rate(Figure 5.5, 5.6). It also correlates with Noxon [30] investigations.

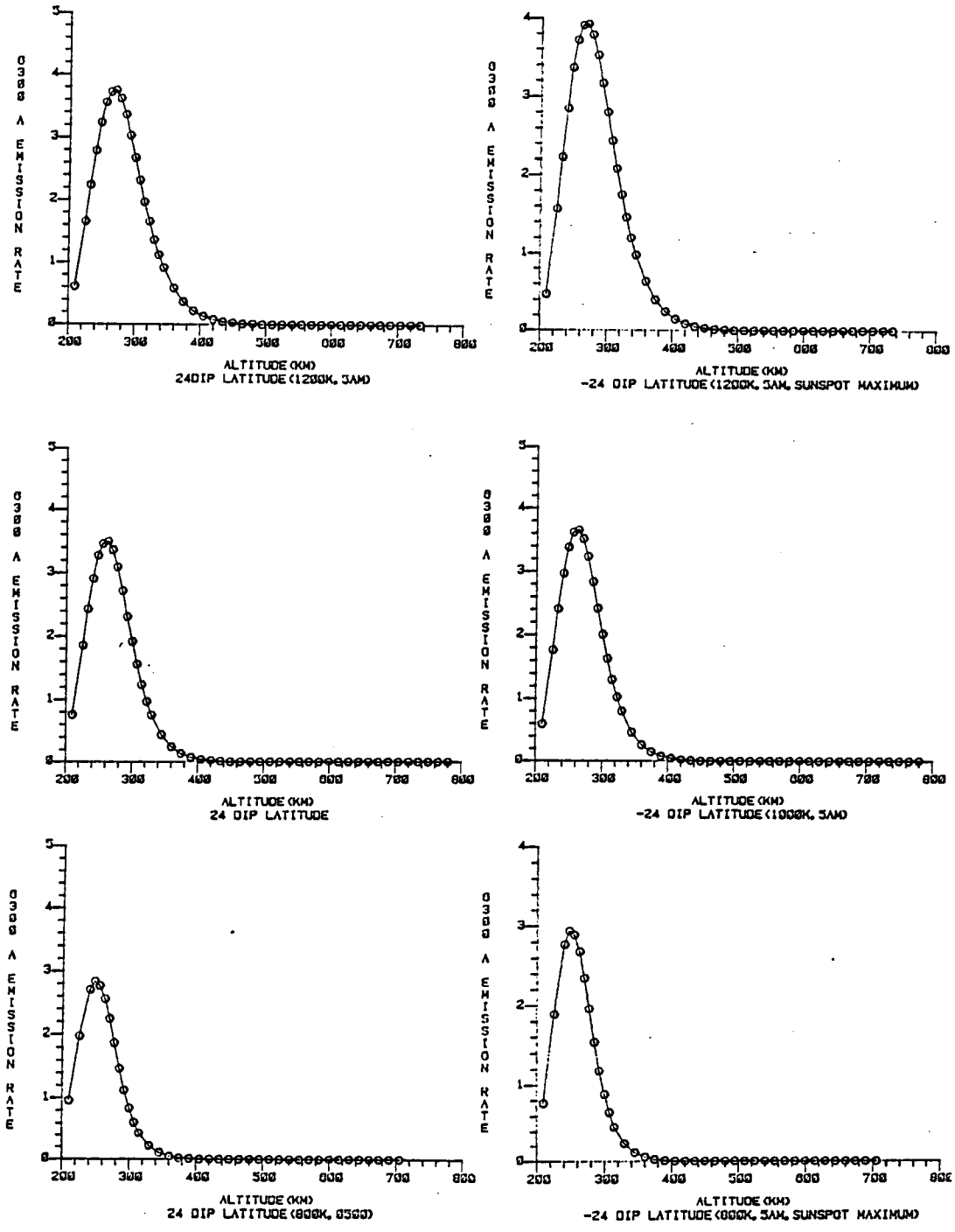


Fig 5.5 Volume Emission Rate Of Oxygen At 6300Å Versus Altitude For Sunspot Maximum, Equinox Season At 0500 LT.

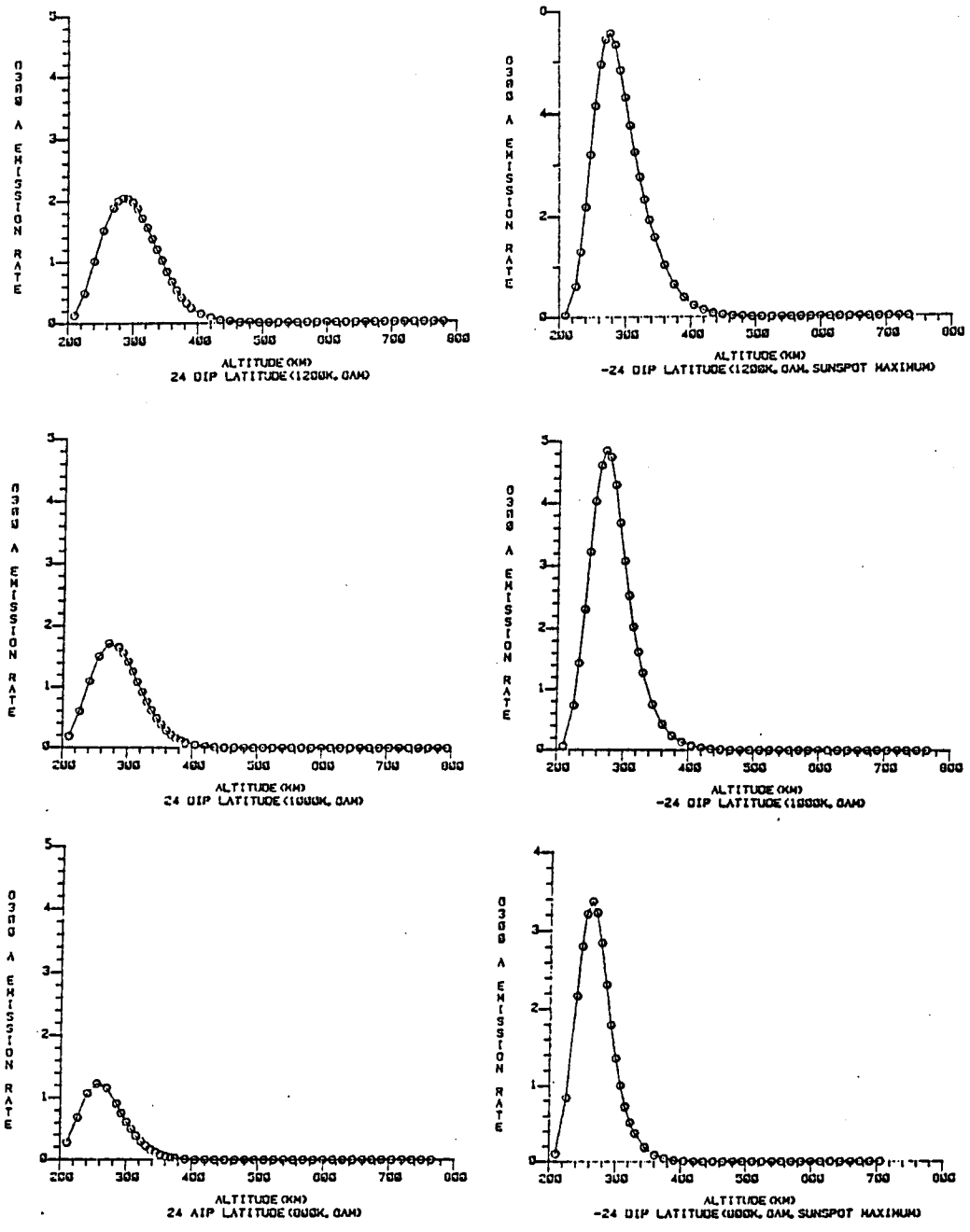


Fig 5.6 Volume Emission Rate Of Oxygen At 6300Å Versus Altitude For Sunspot Maximum, Equinox Season At 0600 LT.

5.3 EMISSION RATES OF OXYGEN AT 1356Å AND 7774Å

Ultraviolet emissions of OI at 1304Å ,1356Å and near infrared emissions at 7774Å in the region of Appleton anomaly can be used as a way of remotely sensing F region and exosphere plasma properties, and the winds responsible for plasma transport. The recent development in the theory of F region and exosphere plasma processes radiative recombination and ion-ion recombination are discussed. The radiative recombination results in one material body and a photon, in contrast to dissociative recombination , which results in a two material particles. Thus it is harder to satisfy the need to conserve energy and momentum in radiative recombination than dissociative recombination. Consequently, the rate coefficent for radiative recombination is five times smaller than for dissociative recombination, Hanson [17]. However,in the upper F region, where there are few molecular constituents to produce molecule ions for dissociative recombination, radiative recombination of O^+can be more important. The investigation of OI 1356Å and 7774Å for 53 latitude (26S-26N) reveales that the maximum column emission rate located at $\pm 14^o$ geomagnetic latitude at 2100LT. One appropriate approach to investigate the behavior of Oxygen emission is the Chapman layer model. The Chapman layer model assumes the EDP is always described by a modified Chapman function.This technique make use of the direct relation between atomic oxygen emission features and the oxygen ions.

In the Chapman layer model, the intensities of the two features are related to the EDP maximum, N_{max}, and the height of the maximumn, $h_{max}F_2$ by the equation

$$I_{1356} = g_1(N_mF_2, h_mF_2)$$

I_{1356} is column emission rate and g_1 is a function whose form depends on EDP as

well as chemistry and neutral densities.

$$I_{1356} = I_{ion-ion} + I_{radiative}$$

Premilinary observational results of OI at 1356$\AA$ emissions in the equatorial zone from an experiment abroad the polar orbiting sattelite OGO-4 showed these emissions were most frequently observed during the Equinoxes with maximum intensity around 1400 LT at equator, and it was also shown that the OI 1356$\AA$ emission doesnot correlate with magnetic activity. The 1356$\AA$ distributions reveal that (I+I) recombinations are very significant in the F_1 region after midnight until 0800 LT(Fig 5.7). After 0800 LT, in F_2 region both processes become significant. The maximum column emission rate is 100 Rayleigh at 1400 LT, which about 93 percent is due to radiative recombination, and 7 percent is due to ion-ion recombination. The ion-ion recombination is a maximum at 0900 LT and a minimum at 0600 LT. The minimum column emission rate is 2.21 Rayleigh at 0600 LT, with 1.54, and .671 Rayleigh due to radiative recombination and ion-ion recombination, respectively. OGO-4 predicted the intensity of 1356$\AA$ up to 200 Rayleigh for low latitudes, which correlates with our data.

Calculations of column emission rates does not give an exact relationship in terms of N_{max} and h_{max} in day time of low latitude but at $\pm 21^0$ degree latitude toward the midlatitude, there is a linear relationship between the square root of I_{1356} and electron density and only a weak depedence on $h_m F_2$ as shown in Figure 5.8. The error within 20 percent is acceptable (AFGL[2]). According to our results presented, important expression for the night time F region , Equinox season, solar cycle maximum at critical frequency in terms of I_{1356} can be found.

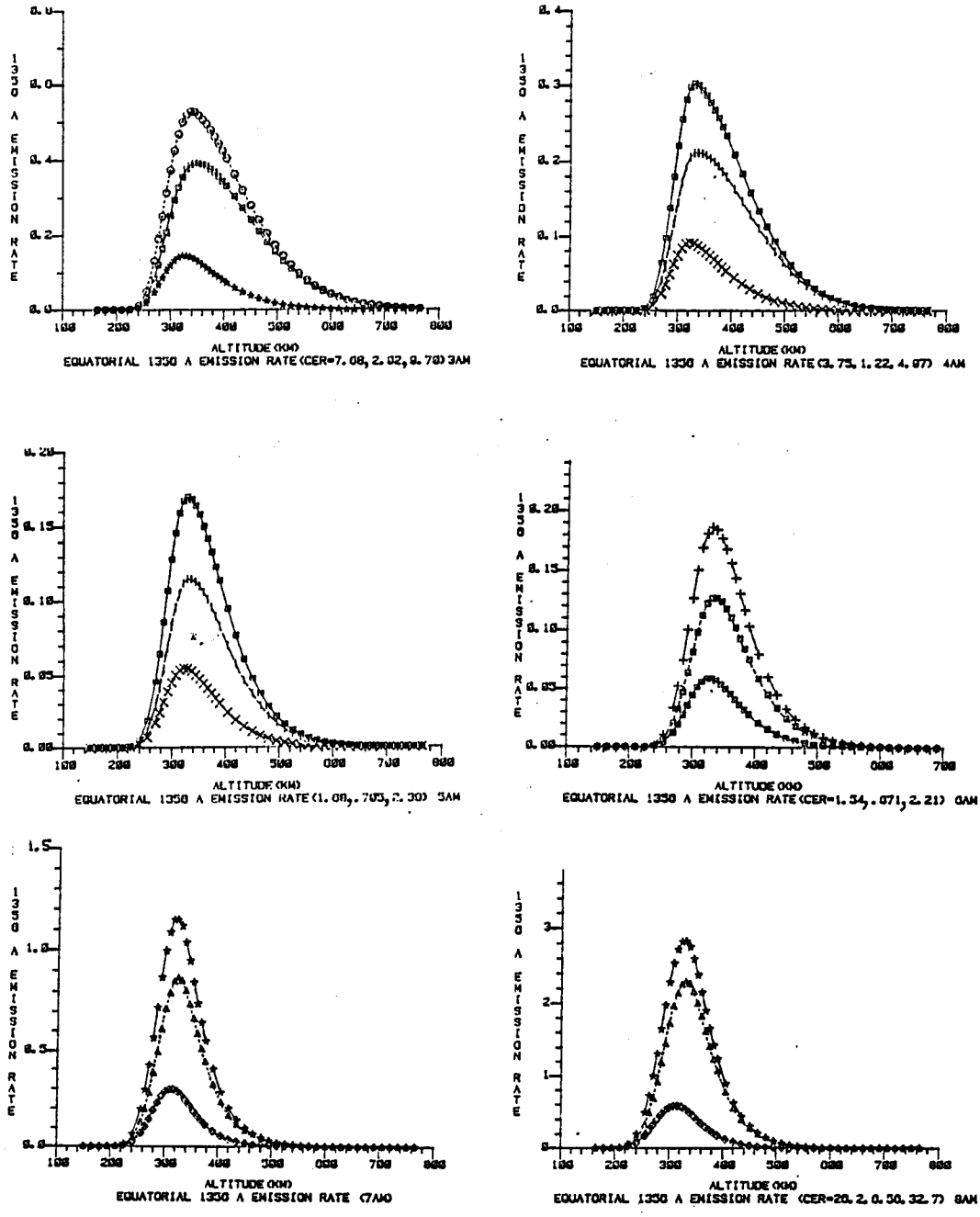


Fig 5.7 Equatorial Volume Emission Rate Of Oxygen At 1356Å Versus Altitude For Sunspot Maximum At Equinox Season.

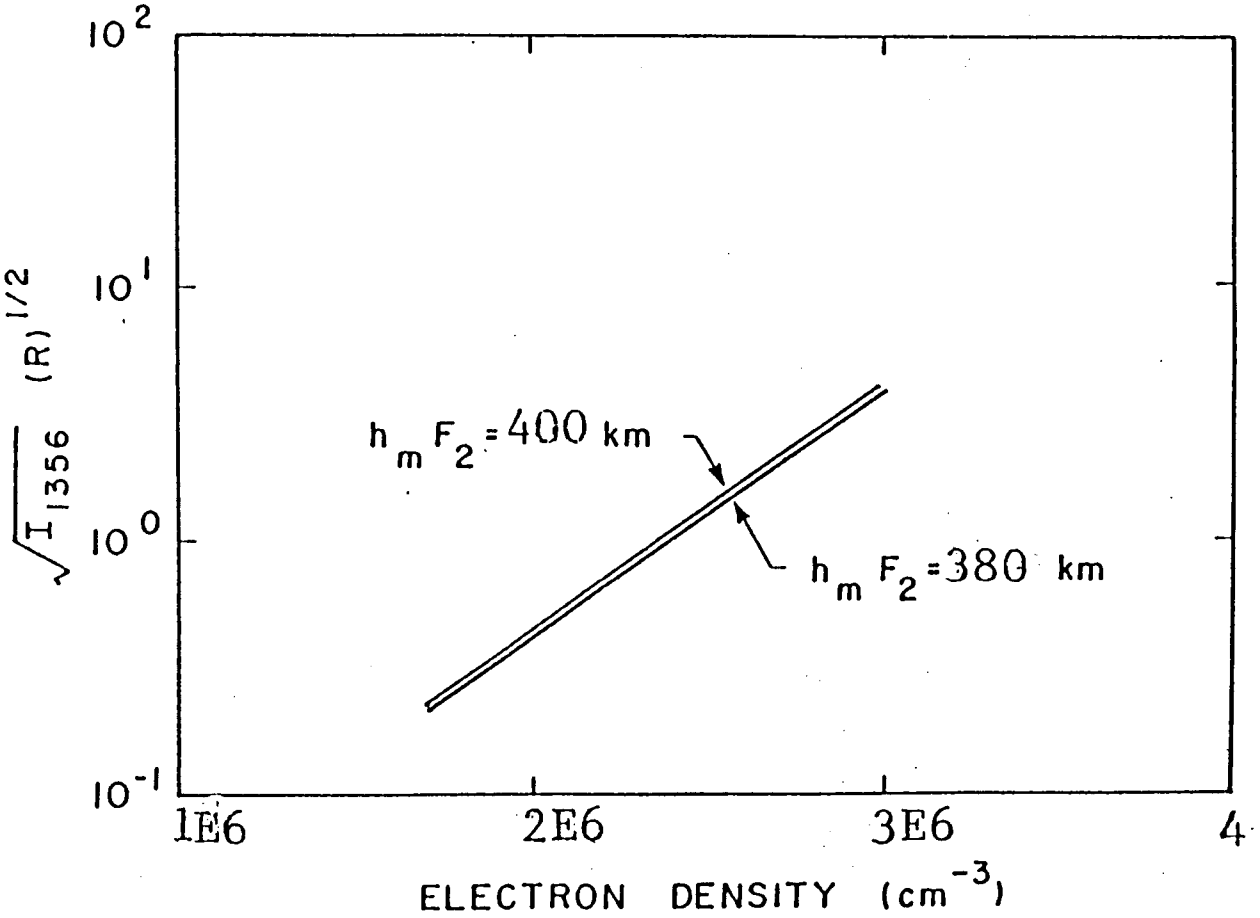


Fig 5.8 The Dependance Of The OI 1356Å Intensity On The N_{max}.

The N_{max} is related to the f_0F_2 according to the expression

$$N_{max}(e) = 1.24(10)^4[f_0F_2]^2 \tag{5.2}$$

where, f_oF_2 is in MHZ and $N_m(e)$is in $\frac{electrons}{(cm)^3}$.

Experimental and theoretical investigations of depleted plasma and their associated irrequlariti es in the equatorial ionosphere, have been made in past few years. Various experimental techniques have been used, including incoherent back scatter radar observations, scintillation measurements , ionosonde measurements, and airglow observations of atomic oxygen at 6300$\mathring{A}$ and 7774$\mathring{A}$. The investigations proposed that ionospheric irrequlariti es at low latitude initially generated through a fluid type, gradient instability mechanisms, and that the ionosperic plasma bubbles are actually plasma depleted magnetic flux tube,(Ossakow[31]). The plasma depleted regions, or bubbles, aligned along the magnetic field lines, are generated in the bottomside of the F region just after sunset, when the layers show rapid movement. These bublles then buoyantly rise upward and westward with respect to ambient plasma, Mcclure[25]. The bubbles are very long and perpendicular to the magnetic plane. They break up in to smaller scale size irrequlariti es which are associated with scintillation and spread F, (Harrendel [18]). The OI 7774$\mathring{A}$ emission can be used to remotely monitor the dynamic of transequatorial bubbles and large scale irregularities in the ionospheric F region.

Measurements of 7774$\mathring{A}$ by Teixeira and Takahashi [38] in Brazil (11.95 S) showed that the peak height, h_mF, can be estimated from the ratio $\frac{I_{7774}^{\frac{1}{2}}}{I_{6300}}$. Moore and Weber [27] discussed that the F layer profile may change from outside to inside of the depletion making the ratio unsuitable for large height determination.

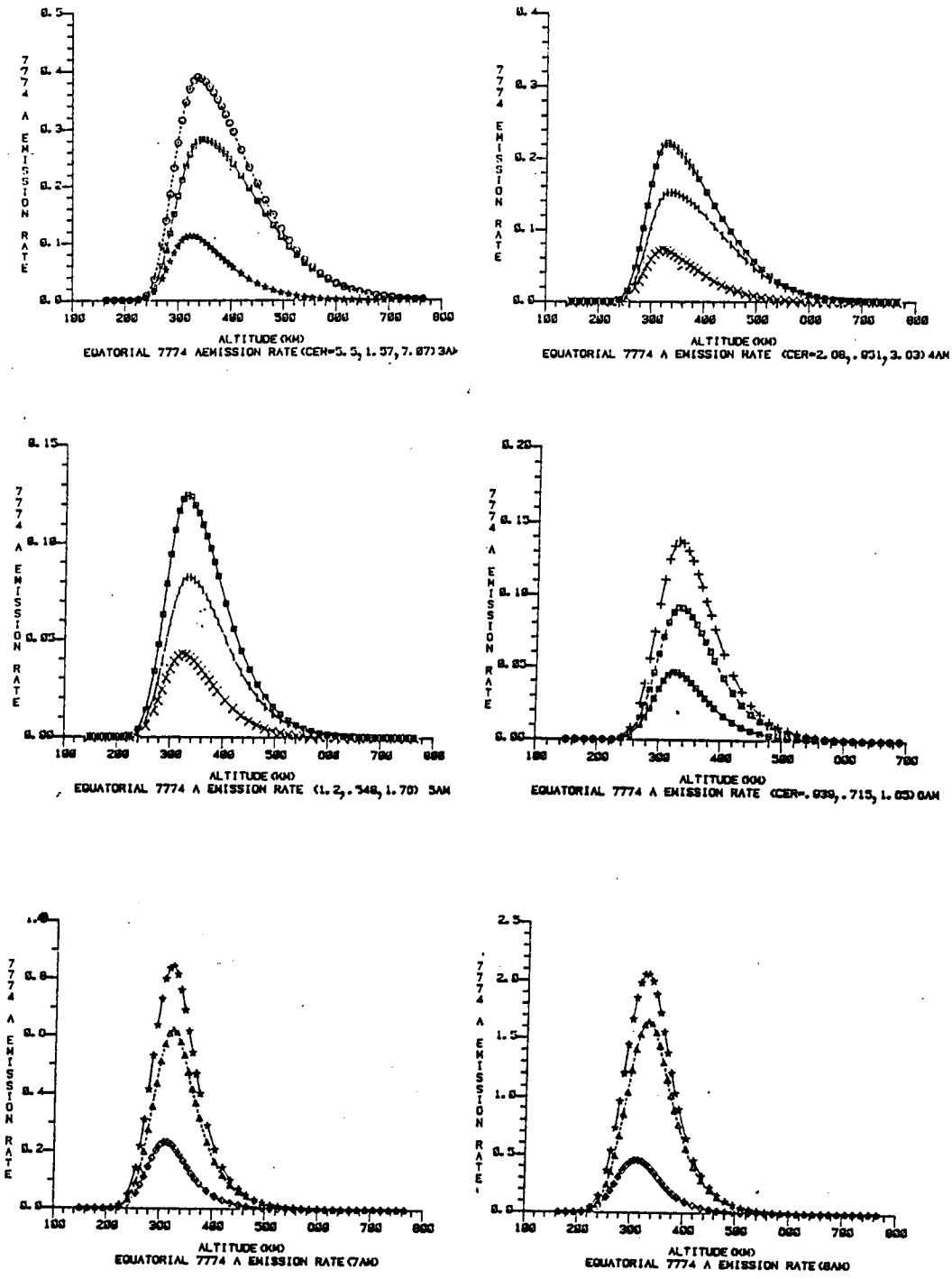


Fig 5.9 Equatorial Volume Emission Rate Of Oxygen At 7774Å Versus Altitude For Sunspot Maximum AT Equinox Season.

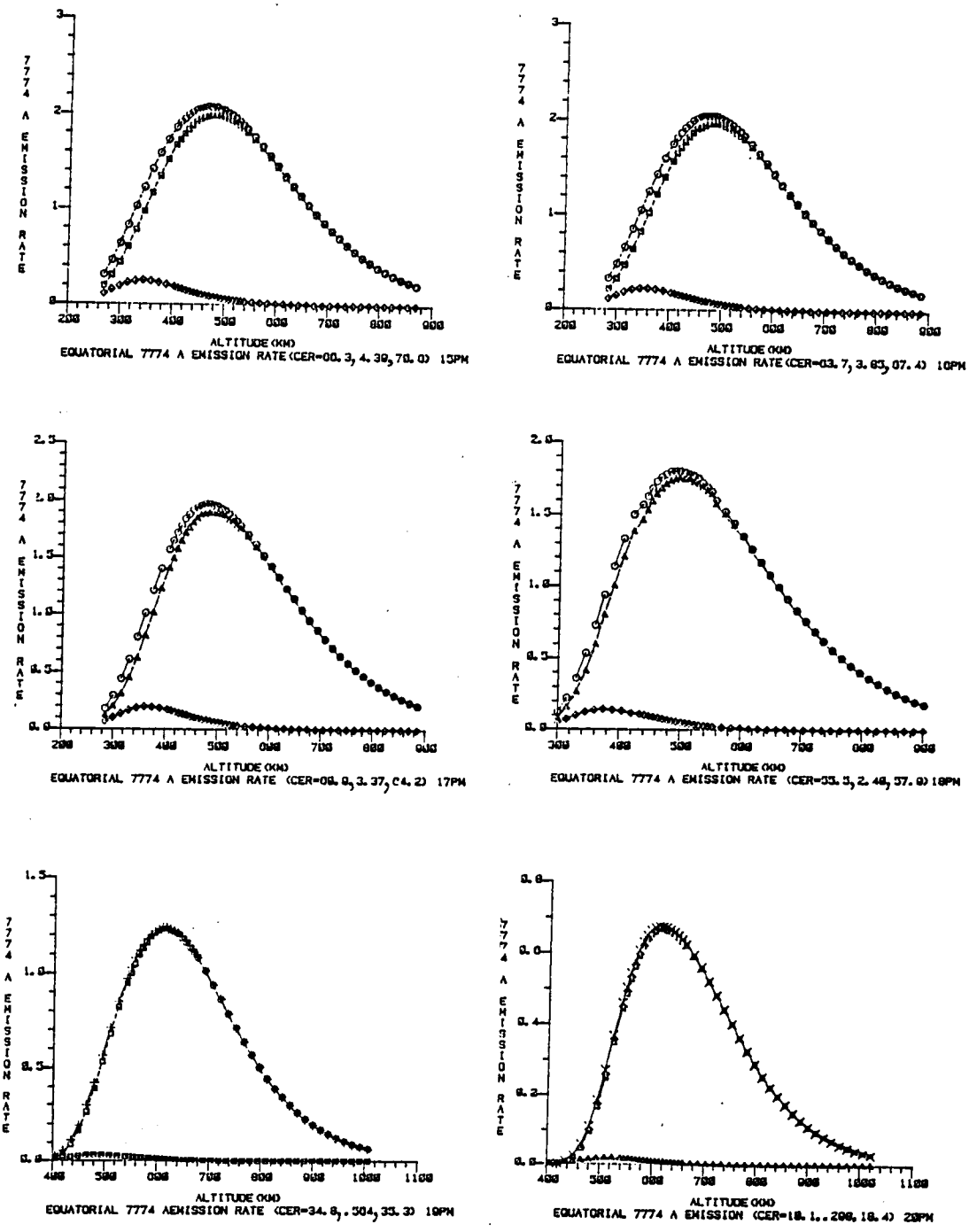


Fig 5.9 Continue.

Figure 5.9 shows the volume emission rate versus altitude at equator. The profiles reveal that roughly 25 percent of total emission rate is due to ion-ion recombination from midnight to 0800 LT. The maximum and minimum column emission rate occurs at 1500 LT and 0600 LT. According to our results, there is no direct relationship between the f_0F_2 and column emission rates at very low latitudes. The intensities depend upon both N_{max} and h_{max}.

Bittencourt, and Sahai [7] in Situ observations by sattelite measured the intensity of the OI 7774$\mathring{A}$ at 22.7 south. According to their results the following expression for the F layer in terms of critical frequency obtained at night.

$$f_0F_2 = [430I_{7774}]^{\frac{1}{4}} \tag{5.3}$$

The observed intensities can be related to N_{max} when there is no spread F. In the case of spread F, the depression seen in f_0F_2 values, reflects a decrease in integrated vertical electron density.

The above equation correlates with our investigations from -20 to -26 degrees latitude with error about 15 percent in $N_{max}F_2$ and almost error about 26 percent from 20 to 26 degrees latitude.

One of the major factors that one need to consider in order to generate a realistic volume emission rate, is particle precipitation as discussed by Hicks and Chubb [20]. The problem with particle precipitation is that any exciting electron would have to have an energy of about 10 ev to produce the right ratio of spectral lines intensities and to fail to excite lower altitude constituents such as molecular nitrogen. As one can observe the particle precipitation may have substantial influence in total emission rates.

5.4 EMISSION OF OXYGEN AT 911$\AA$

The oxygen at 911$\AA$ is direct recombination to the ground state.The maximum column emission rate occurs at either side of geomagnetic latitude at ± 14 degree latitude (2100 LT). The maximum and minimum column emission rate is 43.5 and .723 Rayleigh at equator as shown in Fig 5.10. The OI 911$\AA$ from OGO-4 showed that the intensity is proportional to $f_0 F_2^4$ or they correlate with N_{max}^2. These results correlates with our data at night after the enhancement of the maximum electron density.

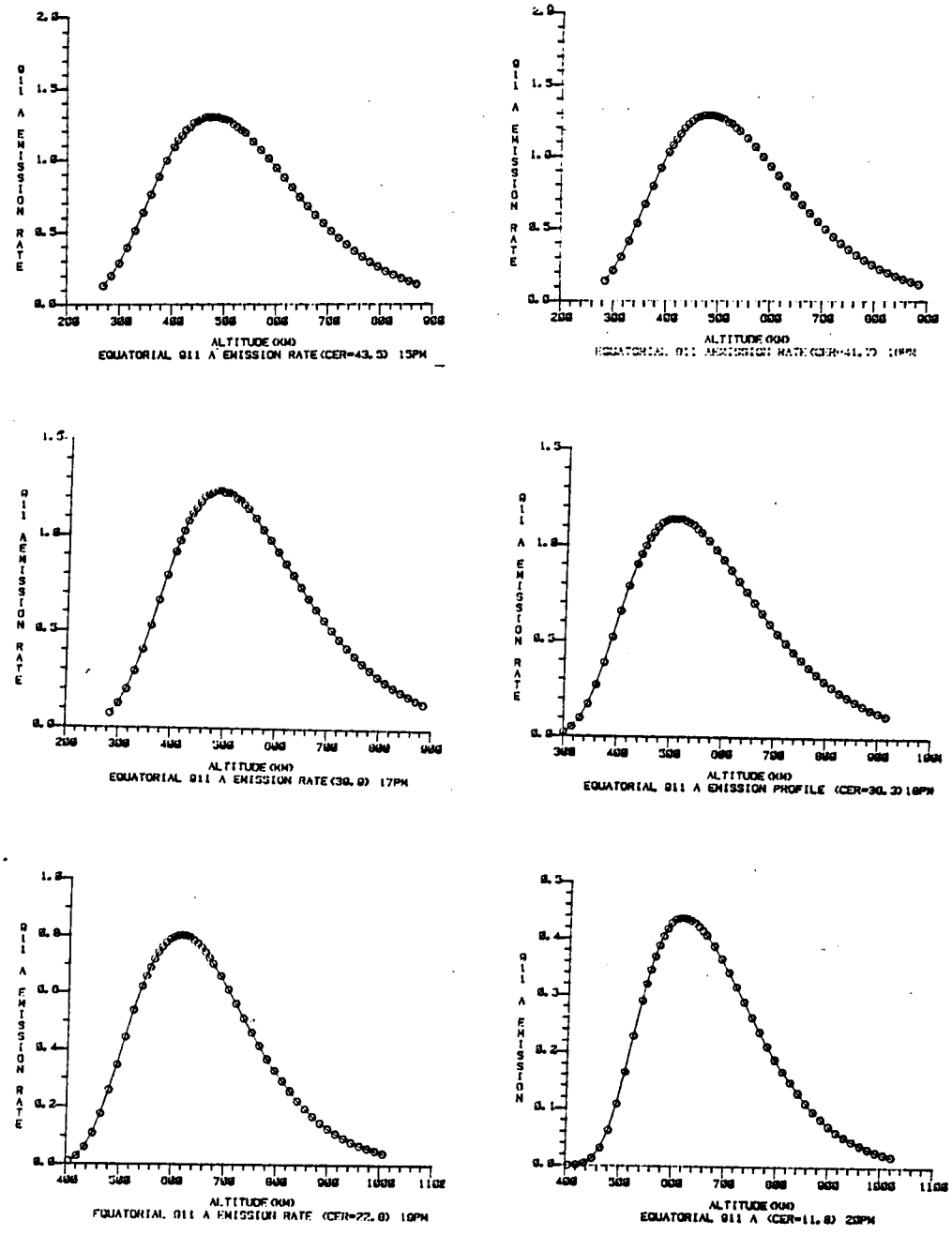


Fig 5.10 Equatorial Volume Emission Rate Of Oxygen At 911Å Versus Altitude For Sunspot Maximum At Equinox Season.

CHAPTER 6

CONCLUSION

The investigation of low latitude electron content in F region and exosphere plasma reveales that one can define the Appleton anomaly for sunspot maximum at equinox season in a new fashion. The investigation shows that the total electron content reaches its maximum development at 2100 LT with the crest nearest the equator being the greatest. This asymmetry reverses at 0200LT when the crest farthest form the equator is smallest. The noon bite out occurs at 1200 LT and continues until the night. The total electron content does not change significantly at 1400 LT, 1600 LT, 1700 LT. The sharp drop in total electron content can also be considered a sign that the F layer is rising rapidly after sunset and equatorial spread F is likely to happen.

The dynamic interaction between the neutral and ionized gas is discussed. The neutral wind which blows toward the equator is large before midnight because of reduced ion drag. As the layer descends, the increase of ion drag causes the neutral wind to decrease. Through the continuity the convergence of the neutral wind results in a downward vertical motion and causes the temperature pertubation around midnight. The temperature pertubation changes the electron number of density.

The neutral winds which blow from north to south transport ionization from the northern hemisphere to the southern hemisphere causing $N_{max}F_2$ to be larger in the south initially. But because the neutral wind also causes $h_{max}F_2$ to be at a lower altitude in the south where the loss rate is greater, the ionization at night decays

faster in the southern hemisphere, causing a reversal in the asymmetry of $N_{max}F_2$ and TEC. Because of the competing mechanisms of transport, production and loss, the important processes affect the time dependent electron density distribution and total electron content.

The meridional winds which blow from south to the north tend to move the ionization upward to the south and downward to the north. In this situation F_2 peak will be higher south of the equator resulting in asymmetrical distribution in the airglow emissions. In addition, thermospheric winds significantly affect the structure of ionospheric plasma dynamics.

An understanding of the asymmetry in emission rates and electron densities are very complicated. The problem require a comprehensive investigation about the global pressure gradients, which is the driving force for the ionospheric winds.

The comparison of the model with the observations using the Jicamarca incoherent scatter radar facility demonstrates that h_{max} at 2000 LT and 1400 LT are in reasonable agreement. Again, these profiles vary with vertical $\overline{E} \times \overline{B}$ drift velocities whose diurnal variations may have significant day to day changes .

The ion-ion and radiative recombination processes in the F region and exosphere plasma are compared. It appears that ion-ion recombination contributes significantly to the calculated total tropical ultraviolet airglow, but the contribution will not exceed that due to radiative recombination. The continuum radiation arising from electron attachment to atomic oxygen would provide an upper limit to the ultraviolet radiation that could result from ion-ion recombination. The investigation of OI radiation in the far ultraviolet and near infrared have provided a new means of studying the equatorial anomally. The emissions will be important to study the dynamics of the large scale irrequlatities and the generation processes of the transequatorial bubbles. The bubbles aligned along the geomagnetic field lines

are generated in the F region and exosphere plasma just after sunset, when the layer shows a rapid upward movement. The investigation shows that the square root of intensity at 7774$\AA$ to oxygen intensity at 6300$\AA$ can not determine the height of the $h_{max}F_2$ uniquely. Therefore, it depends to electron density profiles. The F layer profiles change from outside to inside the depleted region(or bubbles) making this ratio unsuitable for layer height determination.

A modified chapman layer is introduced to investigate the emission of oxygen at 1356$\AA$. It appeares that the square root of OI 1356$\AA$ varies linearly with N_{max} from $\pm 21^o$ toward mid latitude at night. The maximum intensity occurs at $\pm 14^o$ latitude.

The OI 911$\AA$ is direct recombination to ground state. The OI 911$\AA$ behaves like $f_0 F_2^4$ after the enhancement of the maximum electron density. The maximum intensity appears to be at $\pm 14^o$ latitude.

The OI 6300$\AA$ is the brightest dayglow source. It appears that OI at 6300$\AA$ is strongly a function of N_{max} andh_{max}. The maximum intensity occurs at $\pm 13^o$ latitude at 0200 LT. The investigation shows that the crests move from 20^o at sunset to 8^o at midnight on the average. The minimum of OI emission falls to 4^o latitude at 1700 LT. Good fits have been obtained between observed airglow intensities and our calculations. The radar measurements show that a significant portion of the emission comes from the above F layer peak, thereby making it difficult to perform precise calculations with ionosonde data. The data shows that the latitudinal asymmetry is associated with asymmetry in the height of the OI 6300$\AA$ emission and hence with the altitude of the F_2 peak.

CHAPTER 7

RECOMMENDATIONS

As our investigation indicatens that one of the important future roles that theoretical ionospheric models can play is to improve our understanding of the various coupling processes which occur between:

1. Plasma density and plasma temperature.
2. Electric fields, neutral winds and plasma density as it applies to both large scale ambient ionosphere and to the growth of smaller scale structures.
3. Ionosphere-plasmasphere coupling at low latitudes.
4. Electron density across the depleted region.
5. Spread F and electron density height.
6. particle precipitation and OI emissions.
7. Low energy electrons from magnetic conjugate point and OI at 6300$\mathring{A}$.
8. Pressure gradients and the ionosperic winds.

Understanding the feedback processes which occur among the various relevant physical processes will allow us to progress beyond the stage of adjusting input parameters so that calculated ion and electron density matches the observed values. These are not easy problems to solve and extensive further ionospheric investigations are required.

BIBLIOGRAPHY

BIBLIOGRAPHY

1. Abur, M. F., and D. W. Windle (1969). "The Day And Night Reversal In The N_mF_2 North South Asymmetry," Planet Space Science, 97.

2. AFGL (1985)." Determination of Ionospheric Electron Density Profiles From Sattelite UV Emission Measurements FY84,"913, April.

3. Anderson, D. N. (1981)." Modeling the Ambient, Low Latitude F Region Ionosphere," Journal of Atmospheric and Terrestial Phy, October.

4. Appleton, E. V. (1946)." Two Anomalies In The Ionospere," Nature , 157.

5. Bates, D. R. (1962)." Atomic And Molecular Processes," Academic Press , 57.

6. Bent, R. B. (1973)." Documentation And Description Of The Bent Ionospheric Model," AFCRL TR. 73, June.

7. Bittencourt, N. R., and Y. Sahai. (1983)."Observations of Large Scale Irrequlariti̊es Using The Airglow Emissions at 7774Å and 6300Å ," Annales Geophysicae.

8. Caruthers, G.R., and T. L. Page. (1972)."Applo 16 Far Ultraviolet Camera, Earth Observations," Science, 177, July.

9. CCIR. (1978)."International Telecommunication Union,"AFGL-TR 85, October.

10. Chandra, S. (1970)."OGO-4 Observations Of Ion Composition In Topside Ionosphere,"Journal Geophy Res, 75.

11. Chapman, S. (1956)."The Upper Atmosphere Physics, "Proc. Phy. Soc. 43, 26 , 484.

12. Dalgarno, A, and M. B. Mccelroy. (1983)."Electron Impact Excitation Of The Dayglow,"J. Atmos. Sci, 26.

13. Dickenson, R. E., R. G. Roble. (1979)."Thermospheric Motion and Temperature Pertubations,"Space Res , 13.

14. Fejer, B. G. (1982)."Dependance Of The Equatorial F Region Vertical Drifts On Season And Solar Cycle,"J. Geophy. Res, 84.

15. Forbes, J. R. (1982)."Atmospheric Tides,"J. Geophys. Res, 87.

16. Goldberg, R. A. (1974)."Tropical Airglow Of Oxygen,"J. Geophy. Res. 4.

17. Hanson, W. B. (1970)."A Comparison Of Oxygen Ion-Ion Neutralization And Radiative Recombination Mechanisms For Producing The Ultraviolet Nightglow,"J. Geophy. Res, 75.

18. Harrendel, G. T. (1973)."Comparison Of Optical Incoherent Scatter And Jacchia Model Neutral Temperatures In The Night Time Equatorial F Region," EOS Trans. Agu, 54, january.

19. Harris, I., and W.Priester.(1962)."Time Dependant Structure Of The Atmosphere," J.Atmos Sci, 19.

20. Hicks. G. T, and T. A. Chubb.(1970)."Equatorial Airglow In The Far Ultraviolet and Near Inferred," J. Geophy. Res, 75.

21. IRI. (1981)."International Reference Ionosphere," World Data Center, NOAA, 179.

22. Johanson, F. S. (1956)."Temperature Distribution Of The Ionosphere Under Control Of Thermal Conductivity," J.Geophy. Res, 61.

23. Kendell, P. C. (1967)."Magnetoplasma Diffusion At F Region Altitudes," Planet. Space Science, 15.

24. Knudsen, W. C. (1970)."Tropical Ultraviolet Nightglow," J. Geophy. Res, 71.

25. Mcclure, J. P. (1979)."Ionization Transport Effects In The Equatorial F Region," J.Geophy. Res, 71.

26. Moffet, R. J. (1979)."The Equatorial Anomaly In The Electron Distriution Of The Terrestrial F Region." Fund. Cosmic Phys. 4.

27. Moore, J. G, and E. J, Weber. (1981)."OI 6300 and 7774 Airglow Measurements of Equatorial Plasma Depletions,"J. Atmos Terrest. Phy,43.

28. MSIS, (1983)."A Revised Thermospheric Model Based On Mass Spectrometer And Incoherent Scatter Radar,"J. Geophy. Res, 88.

29. Narcisi, R. S. (1981)."Direct Measurements Of Electron Density, Temperature and Ion Composition In An Equatorial Spread F Ionosphere,"J. Atmos Terrest.Phy, 43.

30. Noxon. J. F. (1975)."Interpretation of F Region Nightglow,"Astrophysical . J, 54.

31. Ossakow, S. L., and S. T, Zalesak. (1979)."Nonlinear Equatorial Spread F , Dependance on Altitude Of The F Peak,"J. Geophy. Res, 84.

32. Peterson, V. L.,and T. E, Van zandant. (1969)."O^1D Quenching In The Ionospheric F Region,"Planetary Space Science, 17.

33. Pickering, W. M., and P. C, Kendall. (1967)."Diffusion At F_2 Region Altitudes,"Planetary Space Science,15.

34. Rishbeth, H. (1971)."Polarization Fields Produced By Winds In The Equatorial F Region,"Planet Space Science, 19.

35. Roble, R. G., and R. E. Dickenson. (1974)."The Effect Of Displaced Geomag-

netic And Geographic Poles On The Thermospheric Winds," J.Planet Space Science, 22.

36. Sahai, Y., and J. A, Bittencourt., and H, Takahashi. (1981)."Plasma Irrequlari-ties In The Equatorial F Region Detected By OI 7774Å and 6300Å Nightglow Emissions," J. Geophy. Res, 86.

37. Schaeffer, B.C., and P. D, Feldman. (1972)."Dayglow 6300Å and 5557Å Lines In The Early Morning Ionosphere," J. Atmos, phy, 15.

38. Teixeira, N. R., and H. Takahashi. (1983)."Observations Of Large Scale Irre-qularities In F Region," J. Atmos. Terrest. phy, 43,May.

39. Torr, M.R., and D. G, Torr. (1979)."Chemistry Of The Thermosphere and Ionosphere," J. Atmos. Terrest. Phy,41.

40. Van zandat, T. D., and A, Tinsley. (1970)."Theory Of F Region Processes ,"J. Geophy. Res, 21.

41. Rastogi, R. G. (1978)."Irrequlariti es In Upper Atmosphere And Spread F,"Proc. Indian Acad Science, 87.

42. Woodman, R. F. (1970)."Vertical Drift Velocities And East-West Electric Fields At The Magnetic Equator,"J.Geophy. Res, 75.

43. Zipf, E. C. (1970)."The Dissocuative Recombination Of O_2 Ions In to Specifically Identified Final Atomic States,"Bull. Amer, soc, phy, 15.

VITA

Cyrus Aghanajafi was born in Tehran-Iran. He graduated from the Alborz high school with a major in mathematics and physics on April 1978. Shortely after he came to the United States for college education. He received his BS and MS in mechanical and civil engineering on June 1984. Cyrus joined the University of Tennessee Space Institute as a Grduate Research Assistant on September 1984. He was involved in several projects such as second law analysis using available energy concept for compressible and incompressible flow, electron density in ionosphere and their applications for satelite communications, emissions of different bands of oxygen to design sensors for satelites and investigation of the space station environment. Cyrus completed the requirements for PhD in mechanical engineering with speciality in space sciences (engineering) on June 1988.